공학박사 학위논문

선택적 촉매 환원법을 위한 요소수용액의 증발과 분해에 관한 연구

A study on evaporation and decomposition of aqueous urea for Selective Catalytic Reduction technology

2016년 2월

서울대학교 대학원

기계항공공학부

단 호 진

선택적 촉매 환원법을 위한 요소수용액의 증발과 분해에 관한 연구

A study on evaporation and decomposition of aqueous urea for Selective Catalytic Reduction

지도 교수 이 준 식

이 논문을 공학박사 학위논문으로 제출함
2015년 10월

서울대학교 대학원
기계항공공학부
단 호 진

단호진의 공학박사 학위논문을 인준함
2016년 2월

위 원 장 _____ (인)

부위원장 _____ (인)

위 원 _____ (인)

위 원 _____ (인)

위 원 _____ (인)

A study on evaporation and decomposition of aqueous urea for Selective Catalytic Reduction technology

Ho Jin Dan

School of Mechanical and Aerospace Engineering

The Graduate School

Seoul National University

Abstract

Air pollution has serious impacts on the environment and health. One of main sources that cause the air pollution is the emission from internal engines burning fossil fuel. Urban area is more vulnerable due to dense vehicle density so that countries around the world set up emission standards to cope with the situation. Since nitrogen oxides produced during high-temperature combustion cause photochemical smog and acid rain in the atmosphere, the emission standards make a strict restriction on NOx emission. Engine manufacturers have been developing technologies to meet the regulations. One of practically available ways to meet the regulations is a technology of selective catalytic reduction using aqueous urea (Urea-SCR).

Urea-SCR technology uses aqueous urea that should be converted into ammonia in the exhaust stream because ammonia is used as a reducing agent in the SCR catalyst. Water evaporation, urea

hydrolysis and hydrolysis of isocyanic acid take part in the converting processes. These processes begin with the sprayed injection of urea in the stream. Some of injected droplets reach the surface of the channel and form deposits. This study is a fundamental research on chemical reactions and thermos-physical properties of urea and its role in the water solvent to understand the deposit formation.

A urea pyrolysis model for temperature around 200℃ where most deposition takes place in SCR systems is presented. The reactions and their chemical kinetics among primary species such as urea, isocyanic acid, biuret, cyanuric acid, and ammonia are proposed. A two-step numerical scheme based on the model is also developed to track molar history of species. The kinetic parameters of the model are obtained by comparing measured masses with simulated ones to minimize the sum of squared errors between them. The present model is able to anticipate the amount of cyanuric acid which is a main ingredient of deposits for the temperature around 200℃ and forms polymeric complexes at higher temperature. Kinetic coefficients for urea pyrolysis are compared with other authors' results to validate the model. The competition between the formation of cyanuric acid and the evaporation of isocyanic acid is shown a key factor for product deposits which can be filed up more at lower temperature.

Water vaporization from aqueous urea is a first process during the conversion of urea into ammonia. Droplets sprayed into the exhaust gas stream are composed of non-volatile urea solute and water solvent. As water evaporates, relative composition and thermo-physical properties of the solution change. It is called a colligative property. Two colligative properties to understand water evaporation are boiling-point elevation and change in heat of vaporization of water from aqueous urea. The boiling-point elevation relation for water in the mixture is derived and shown to be valid by experiments. The heat supply to droplet from the surrounding gas and its distribution to

evaporation, heating evaporated vapor, and heating droplet are analyzed using the proposed boiling-point elevation relation. The change in enthalpy of vaporization of water from aqueous urea is calculated considering endothermal heat for urea dissolution in water. The change is validated by experiments as well. Droplet evaporation analysis reveals that droplet temperature can increase high enough to begin urea decomposition. Since droplets convey energy to wall and their precipitation is related to drop temperature, the proposed model will be useful for calculating drop temperature and species fractions in Urea-SCR system design.

Keyword : Urea-SCR, Urea pyrolysis, Water evaporation, Cyauric acid, Boiling-point elevation, Heat of vaporization
Student Number : 2012-30170

Table of Contents

List of Tables

List of Figures

List of Codes

Nomenclature

Roman symbols

A : Area

A : Pre-exponent factor in A_i

B_T : Spalding heat transfer number

c : Molar concentration [mol/ml]

c : Specific heat of mixture

$\bar{c}$: Average specific heat of mixture

C_D : Diffusivity as in D_g

c_p : Specific heat for gas at constant pressure

D : Diameter as in D_d

D : Diffusivity as in D_g

E_a : Activation energy

F : Force

f_Δ : Sourcing term form the reaction of biuret equilibrium

g : Gravitational acceleration constant

h : Urea film depth

ΔH : Heat of vaporization of pure water

$\Delta H'$: Heat of water vaporization of water in the mixture

k : Kinetic constant in k_i

k : Thermal conductivity in k_g

Le : Lewis number

m : Mass

n : Molar quantity

M : Molecular weight

Nu : Nusselt number

P : Pressure

Pr : Prandtl number

$\dot{Q}$: Heat transfer rate

R : Gas constant

Ra : Rayleigh number

Sh : Sherwood number

t : Time

t^* : Scaled time

T : Temperature

ΔT : Temperature increment/elevation

x : Mole fraction

Y : Mass fraction

Greek symbols

α : Thermal diffusivity

β : Kinematic constant for effusion process

β : Thermal expansion coefficient

δ : Incremental quantity

Δ : Incremental quantity contributed by biuret equilibrium

μ : Gibbs free energy

ν : Kinematic viscosity

ρ : Density

Subscipts/superscripts

A : Ammonia

B : Biuret

b.p. : Boiling point

c : Critical point

C : Cyauric acid

d : Droplet

cal : Calculated

DISS : Correction of urea dissolution heat

e : Evaporated

exp : Measured

g : Gas phase/Surrounding gas

I : Isocyanic acid

l : Liquid phase

n.b.p. : Normal boiling point

o : Reference state

pv : Water vapor at constant pressure

s : Except the sensible heat for water vapor

T : Total quantity in solution

U : Urea

W : Water

* : Pure substance

Chapter 1
Introduction

1.1 Background

Nitrogen oxides (NOx) form when fuel is burned at high temperature. NOx is a strong oxidizing gas and it can cause photochemical smog and acid rain in the atmosphere so that emission standards around the world set limits to NOx emissions. One of technical ways to meet the regulations is selective catalytic reduction (SCR). The SCR technology was first applied in thermal power plants in the late 1970s and has been developed to mobile diesel applications.

NOx is chemically reduced into molecular nitrogen and water vapor on the SCR catalyst with help of ammonia as a reducing agent. It is not easy to directly use ammonia for vehicle applications because of storage and handling difficulties due to its high vapor pressure and flammable properties. Its container may explode when exposed to heat. It can also be fatal to humans because of highly toxic and corrosive properties. Aqueous urea as an alternative is used in the SCR system since it is less hazardous and easier to handle than ammonia. However, it is required to be converted to ammonia in the exhaust system of a diesel engine.

In the conversion process, finely sprayed aqueous urea is injected into the exhaust gas stream. Exchanging energies with the exhaust gas, the aqueous urea decomposes into the gas phase ammonia and carbon dioxide. The decomposition of aqueous urea takes place in three steps in the exhaust pipe (Lundstrom et al. (2009); Wang et al. (2009)). Firstly, water evaporates from aqueous urea drop in the urea decomposition process, which is followed by the pyrolysis and hydrolysis of urea to form ammonia and carbon dioxide in the gas

phase, and then they are mixed with the products of combustion and fed on the SCR catalyst. The reactions in the stream are summarized as follows:

$$NH_2-CO-NH_2\ (aq) \rightarrow NH_2-CO-NH_2\ (s) + xH20 \quad (1.1)$$

$$NH_2-CO-NH_2\ (s) \rightarrow NH_3\ (g) + HNCO\ (g) \quad (1.2)$$

$$HNCO\ (g) + H_2O \rightarrow NH_3\ (g) + CO_2\ (g) \quad (1.3)$$

However, some of the injected droplets of aqueous urea impinge on a wall or a mixer of the system and form a film on the surface. The film of aqueous urea follows a different path from the reactions described above in the exhaust system. It could form deposits on the surface to which energy supply from the exhaust gas is not enough to maintain the desirable reactions for producing ammonia. This is one of the challenges for SCR system design to avoid deposit formation on the surface. So far the design has been done based on experimental experience of engineers since there has been no reaction model for deposition to be incorporated into CFD simulations which are impractical to deal with the phenomena with the time order of 10000 s. This is one of the subjects of this thesis and will be dealt in Chapter 2. Urea decomposition model is proposed in the thesis with support of experiments.

As the room for the diesel engine decreases due to the downsizing trend and compact design, it is difficult to assign enough space for the SCR system so that the optimized channel design turns out the be crucial for converting urea into ammonia. So far the CFD simulations are actively used to design the channel to predict ammonia production and mixing quality with combustion products. Ammonia production models have often been developed sacrificing the accuracy of intermediate processes such as water evaporations and urea pyrolysis. Although it is partly because there are not enough

experimental data, it causes difficulty in predicting drop–wall interaction and wall precipitation fouling since the CFD with inaccurate prediction of intermediate processes fails to retrieve the information on the drop temperature and mole fractions of species. This subject will be dealt in Chapter 3. The colligative properties for urea water solution are modeled based on experiments and water vaporization model is proposed in this study.

1.2 Emission Regulations

Air pollution has serious impacts on the environment and health around the world, particularly in urban area. Since one of major contributors that cause the pollution is the combustion of fuels from vehicles, engine emission regulations are set to limit harmful emissions to be released in the air. Emissions of nitrogen oxides, total hydrocarbon, non–methane hydrocarbons, carbon monoxide and particulate matter are regulated, and nowadays the EU set CO_2 per km targets for new cars to encourage for car–makers to manufacture more efficient cars in order to reduce greenhouse gas emissions.

The toxic emission stages in terms of the European standards are referred to as Euro I, Euro II, Euro III, Euro IV, Euro V, and Euro VI for heavy duty vehicles. In Europe the first regulation for diesel engines in heavy duty vehicles was set in 1993 and engine development is driven to meet the successive regulations. Table 1.1 contains a summary of the emission standards and their implementation dates.

Diesel engine manufacturers try to develop more fuel efficient engines with after treatment systems to reduce the emission of particulate matter (PM) and nitrogen oxide (NOx). Unfortunately, the

Diesel Dilemma explains how it is difficult to take care of both PM and NOx at the same time. The dilemma came from the fact that when the combustion is designed for low NOx emission, PM will be high and vice versa. Although this study is related to NOx treatment by the SCR technology, it should be considered the impact of technology for reducing NOx on PM emission sooner or later.

Table 1.1 EU Emission Standards for Heavy-Duty Diesel Engines: Steady-State Testing

Stage	Date	CO	HC	NOx	PM	PN	Smoke
		g/kWh				1/kWh	1/m
Euro I	1992, ≤ 85kW	4.5	1.1	8	0.612		
	1992, >85kW	4.5	1.1	8	0.36		
Euro II	1996.1	4	1.1	7	0.25		
	1998.1	4	1.1	7	0.15		
Euro III	1999.10 EEV only	1.5	0.25	2	0.02		0.15
	2000.1	2.1	0.66	5	0.10[a]		0.8
Euro IV	2005.1	1.5	0.46	3.5	0.02		0.5
Euro V	2008.1	1.5	0.46	2	0.02		0.5
Euro VI	2013.01	1.5	0.13	0.4	0.01	8.0×10^{11}	

PM = 0.13 g/kWh for engines < 0.75 dm^3 swept volume per cylinder and a rated power speed > 3000 min^{-1}
PN = Particulate number standard
Smoke = Smoke Opacity is the degree to which smoke blocks light
EEV = Enhanced environmentally friendly vehicle

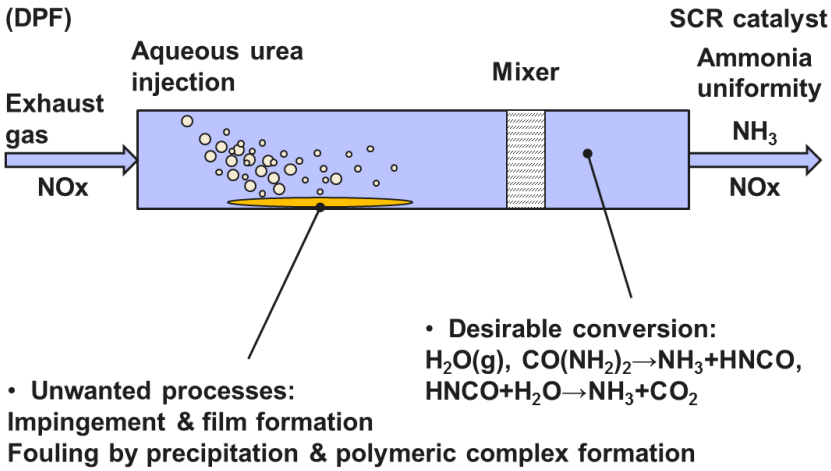

Figure 1.1 Processes before the SCR catalyst

1.3 Simulation for Urea-SCR Technology

Simulation is actively conducted to design Urea-SCR systems. There are two key simulation areas: Process analysis before the SCR catalysis and reactions over the catalyst. The latter uses empirical or physico-chemical reactor models to describe catalytic NOx reducing processes which are out of this research scope. For the process analysis in the exhaust channel before the catalyst, Computational Fluid Dynamics (CFD) is used to mainly evaluate ammonia uniformity at the SCR catalyst inlet.

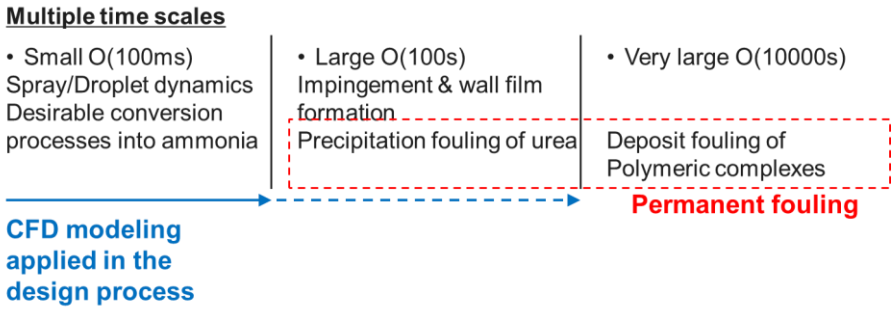

Figure 1.2 Multiple time scales involved in the reactions for ammonia production and fouling processes

As aqueous urea is sprayed into the channel in which the exhaust gas flows. The aqueous urea droplets exchange momentum, energy, and mass with the exhaust or carrier flow. One of the ways that CFD deals with the situation is Eulerian–Lagrangian approach. The carrier flow field is obtained by solving the compressible Navier–Stokes equations including the energy equation in terms of enthalpy. The droplet is treated as a parcel in CFD context which is a representative of the kind. Several models are involved in the simulation for producing ammonia from aqueous urea: kinetics/kinematics for Lagrangian droplet movement, heat transfer model for calculating the amount of energy inflow to drop, and reaction model to change composition in droplets and carrier flow. Droplets also interact with the surface of the channel so that wall film formation model needs to be implemented. The wall film of aqueous urea is also interacting with the environment. It is needed that shear and gravity driven wall film model and energy and mass exchange model are needed. The way of handling droplets is summarized in appendix and some detailed implementation in OpenFOAM is explained.

CFD simulation practice is mainly applied to analyze ammonia uniformity in front of the catalyst. The time scale for the simulation is the order of 100 ms in Figure 1.2. This period of time is not sufficient to know the behavior of wall film. CFD can hardly handle the wall film formation which takes the order of minutes with detailed simulation for spray. It is not possible to get all information for permanent fouling up to the time order of several hours. Besides multiple time scales, there are simulation challenges in Urea-SCR systems since they are related to complex physics. As mentioned before, Eulerian-Lagrangian approach is used to handle multiphase problem with carrier flow in gas phase and droplets in liquid phase. Droplet has evaporating water component with the energy transferred from the surrounding gas. Carrier flow is heterogeneous reacting field as well. Spray and wall interaction due to impingement is challenging subject as well. Most of all, the analysis of Urea-SCR systems is difficult because of lack of validated physical models supported by experiments. It is also hard to simulate whole cycle according to test cycles in emission regulations.

1.4 Purpose of Research

Various elements involves in designing Urea-SCR systems. The main objective of the design is to meet emission standards for NOx emission. Since the Urea-SCR system is not an independent component, its design has influence on the performance of the other after-treatment such as Diesel Particulate Filter. Emission regulations are not the only one objective for the design since the after-treatment system works with sacrificing the efficiency of diesel engine. For example, sprayed urea droplets take energy from the surrounding exhaust gas and the energy would be used in the heat

recovery system such as an organic Rankine cycle. This discussion naturally leads to the optimization of the Urea-SCR system and its interconnected components.

The intra-system-wise optimization can be achieved when the understanding confidence for each individual component is high enough. However as discussed in the previous chapter for the simulation practice, there are elements that are not well revealed or validated by experiments. Despite this level of knowledge, engineers still try to have their objective component as optimized as possible. When it comes to Urea-SCR systems, ammonia supply in front of the catalyst has been a key target though engineers know that various undesirable processes can take place during the urea decomposition to ammonia. Two subjects that are ignored or mistreated so far are addressed in this thesis to extend the formal studies by previous researchers.

The first purpose of this thesis is to reveal the chemical reactions taking place on the wall on the long term of the time order of 10000 s. The reactions which start from the urea decomposition can result in deposit on the wall or internal surface of mixer. A key parameter in the analysis of the reactions is temperature since the wall temperature of the exhaust channel where aqueous urea is sprayed is around the temperature 200℃. The temperature can be dropped further on the surface of the mixer on which cool aqueous urea is heavily impinged. Below the temperature 150℃, the chemical reactions hardly take place and the deposits usually come from the precipitation of urea itself. However, when the temperature is around 200℃, urea decomposition leads to deposits by polymeric complexes. it is hard to remove those complexes unless the temperature reaches 350℃. Since the reactions take long time to finish and they are complicating, engineers don't have proper models to analysis and use an empirical guideline that it should be designed SCR systems

including flow channel to keep its wall temperature over 200℃ during operation. It is however not well known what processes for the deposit formation happen on the wall. Thus understanding urea pyrolysis at the temperature around 200℃ is a first step in the design of a SCR system including dosing control of aqueous urea.

To fulfill the first purpose for the analysis of the chemical reactions related to urea decomposition on the wall, major species are chosen and their chemical kinetics based on the Arrhenius equation and the effusion equation. The reaction model has kinetic parameters to describe the urea decomposition and experiments are performed to obtain the parameters. Once the chemical reactions among key species are obtained, they will be used to deposit analysis on the wall. Mass and heat transfer models will be needed and they are left to further studies.

The second purpose of the thesis is to analysis water evaporation from urea water mixture. Since the formal analysis especially by 3D Computational fluid dynamics (CFD) simulation focuses on the uniformity of ammonia in front of the catalyst. The intermediate processes including water vaporization are not of main interest so that they are often considered as correlating parameters to meet the experimental results for ammonia production. It causes that the temperature information is lost which is important to predict the droplet behavior of aqueous urea when impingement and precipitation fouling. To analyze the vaporization process correctly, thermos-physical properties of the mixture, so called colligative properties should be obtained. There are two colligative properties involved in the water evaporation from the drops of aqueous urea solution: the boiling-point-elevation and the change in the heat of vaporization of water in the solution.

The boiling-point elevation of aqueous urea has not been confirmed experimentally so far to the best knowledge of the author.

An equation is proposed for the binary mixture with non-volatile solute in the solution and validated by boiling experiments. To practical applications, droplet evaporation should be analyzed. With the equation for boiling-point elevation, heat transfer model can be built. Another colligative property is in the way during the heat transfer analysis since the water vapor takes energy to evaporate from the solution and the enthalpy quantity should be precisely known. The enthalpy correction due to urea dissolution in water is investigated. It is not possible to get the accurate behavior of aqueous urea droplet without the enthalpy correction and validated by experiments in the thesis. With the proposed equations for colligative properties, the droplet depletion is investigated in the natural convection and forced convection context. The formal surrounding condition is to compare the prediction with other authors' experiments for single droplet in the controlled hot chamber. The latter is important to show that the proposed models can be incorporated into the CFD code so that they are proved themselves to be practically useful.

Pyrolysis kinetics of urea is described in chapter 2 and the behavior of aqueous urea drop depletion follows in chapter 3.

Chapter 2
Pyrolysis kinetics of urea

2.1 Introduction

The desirable reactions described in chapter 1 in Urea-SCR channel before the catalyst summarized as follows:

$$NH_2-CO-NH_2\ (aq) \rightarrow NH_2-CO-NH_2\ (s) + xH20 \quad (2.1)$$

$$NH_2-CO-NH_2\ (s) \rightarrow NH_3\ (g) + HNCO\ (g) \quad (2.2)$$

$$HNCO\ (g) + H_2O \rightarrow NH_3\ (g) + CO_2\ (g) \quad (2.3)$$

Some of the injected droplets of aqueous urea impinge on a wall or a mixer of the system and form a film on the surface. The film of aqueous urea follows a different path which is the subject in this chapter. It could form deposits of polymeric complexes on the surface when the wall temperature is around 200℃ which is in a usual temperature range by heat exchange with the exhaust gas and the environment.

In the reactions taking place at low temperature on the surface, isocyanic acid plays an important role to form biuret and cyauric acid. The biuret is an intermediate and temporary molecules and it is a reacting species to form the cyauric acid. The cyanuric acid, however, is an ingredient to form polymeric complexes that can contaminate system with deposits. Once deposits are formed on the surface, it is not easy to remove the complexes since they do not decompose below the temperature 320℃ which is not easily attainable on the wall. Like the polymeric complexes, the cyauric acid is hard to remove once it has formed. Moreover, the deposits make it difficult to control ammonia dosing quantity to reduce NOx optimally. Urea overdose is

likely to happen to compensate lack of ammonia due to the deposits and results in accelerating deposition in the system. It could lead to ammonia slip due to the time lag of ammonia generation as well (Fang *et al.* (2003); Strots *et al.* (2009)).

The deposit formation is accelerated when a diesel engine runs with light duty load in low-temperature environments. It is because the surface temperature is low due to lack of energy supply from the exhaust gas and excess of energy loss to the environments. Under such conditions the deposition can be large on the surface since its temperature is hard to be over 200℃ (Strots *et al.* (2009)). It gives an empirical guideline that engineers should design the SCR system including urea decomposition channel to keep its wall temperature over 200℃ during operation. It is, however, not well known what processes for the deposit formation happen on the wall. Thus understanding urea pyrolysis at the temperature around 200℃ will be a first step in the design of a SCR system including dosing control of aqueous urea.

A urea pyrolysis model is proposed for temperature around 200℃. Primary five species are chosen and the chemical reactions among those species are built to describe the behavior of urea pyrolysis. The model is simplified by the way that the reaction for biuret formation would be a relatively fast equilibrium process. Based on the model, a numerical scheme of two-step approach that divides the reactions into slow or fast ones will be introduced to track temporal history of molar quantity of each species. The pyrolysis is expressed in terms of the total mass of the molten mixture that consists of the reactants and products of urea thermal decomposition so that simulated masses can be compared with measured ones. The kinetic parameters of the reactions are obtained from the measured masses and the validity of the model is confirmed by comparing the kinetics of urea thermal decomposition with other researchers. The proposed model aims to

provide with deposit mechanism in the SCR system. It is achieved by the way that the model can anticipate the formation of cyanuric acid which is one of main ingredients and a bridge to polymeric complexes in deposits.

2.2 Experimental apparatus and measurement

A mantle was used to heat 250ml beaker with 70mm in diameter that was employed as an open reactor shown in Fig. 2.1. An in-house controller equipped with K-type thermocouples was used to monitor and control the temperature of the reactor content. Mass was measured by a balance that was separately installed by the side of the mantle.

Aqueous urea was obtained from Grupa azoty distributed with the local name JAVANOX^{TM} in South Korea for automotive applications without any further purification. Urea powder was prepared by evaporating water from the aqueous urea on a hot plate at 85℃ in the glove box with ventilation. Before conducting experiments we heated urea powder again at 85℃ over 30 minutes to remove water from it since it can absorb quite amount of water in the air as time goes on.

Sampling is done once for each urea sample of 20 g. Raw mass data are listed in Table 2.1. Figure 2.1 shows a temperature history of the reactor for the target temperature 180℃. Heat supply to the reactor is controlled to compromise between fast rising time and minimal overshoot of temperature. The fluctuation of temperature is controlled within the standard deviation σ=1.2 K during experiments as shown in Fig. 2.2. In consideration of the phase change of urea a sampling time is calculated by:

$$t = t_3 - \frac{t_1 + t_2}{2} \tag{2.4}$$

Note that during the phase change of urea, the sample temperature was overestimated since the wall temperature affected thermocouples which were put close to the wall where there was not enough molten urea around them at the early stage of heating.

Table 2.1 Raw mass data for urea pyrolysis

Reactor temperature (℃)	Sample mass (g)	Sample time (s)
160℃	17.80	3285
170℃	17.47	2970
	15.98	5940
	14.52	10138
	9.69	terminal①
180℃	15.69	4140
	16.60	2960
	14.69	6390
	13.79	10010
	15.81	4140
	10.387	terminal
190	14.94	3323
	13.76	6120
	11.274	terminal
200	14.45	3025
	11.64	terminal

① 10 to 12 hour-sampling time is used to measure sample mass.

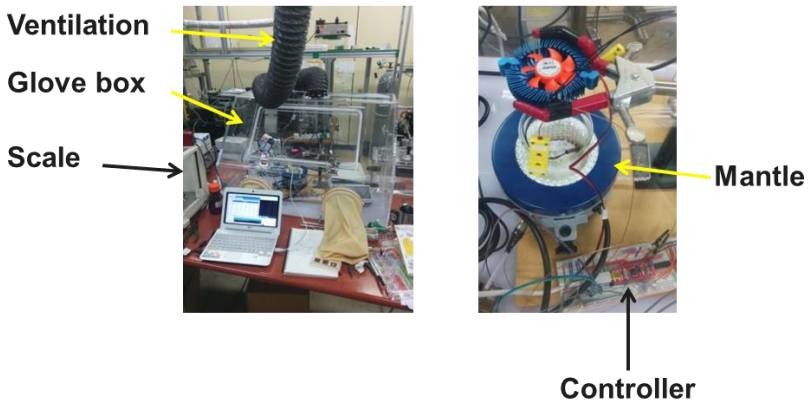

Figure 2.1 Experimental setup

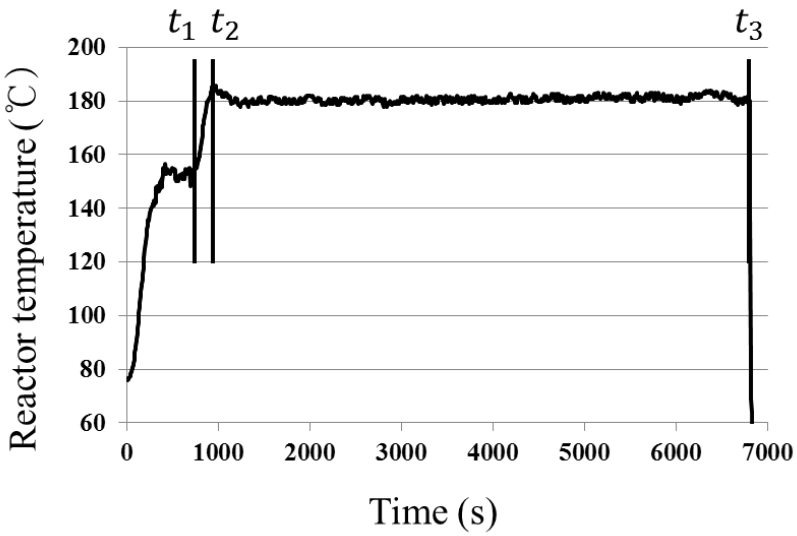

Figure 2.2 A temperature history of the reactor. The initial mass of the sample is 20 g and the target temperature is 180℃. Sampling is done at the time t_3 and sampling time is recovered by $t = t_3 - (t_1 + t_2)/2$ in consideration of the phase change of urea.

2.3 Chemical reactions

It is assumed that there are five species that take part in urea pyrolysis at around 200℃: urea, ammonia (NH_3), isocyanic acid (HNCO), biuret and cyauric acid (CYA). Other species such as triuret, ammelide, ammeline, melamine are ignored because only small traces of form during the urea decomposition (Brack *et al.* (2014)). Cyanuric acid is included not only because its quantity is high but also because it plays a role of gateway to deposit products that cannot be easily decomposed unless the temperature is high enough (Bernhard *et al.* (2012).

There is another assumption on gas solubility. Although ammonia is a polar molecule and dissolves well in polar solutions such as water, it is also known that their solubility goes drastically down as temperature rises. It is not expected that ammonia dissolves in molten urea that can be considered a polar solvent with melting point 133℃ since the vapor pressure of pure ammonia is such large that it is 330 bars at 200℃. Therefore the chemical reaction for urea thermal decomposition is written as:

$$CO(NH_2)_2 \text{ (Urea) (m)} \rightarrow \text{HNCO (l)} + NH_3 \text{ (g)} \qquad (2.5)$$

m in parentheses is used to stress that the reactor has a mixture in molten phase. The phases in the reaction have changed comparing to those of Eq. (2.2). The evaporation of isocyanic acid is modeled separately so that the phase is put liquid in this equation and will be explained shortly. Urea decomposition is assumed a first-order reaction and the kinetic equation for the reaction of Eq. (2.5) is with a kinetic constant $k_1 = A_1 \exp[-E_{a1}/RT]$ from the Arrehnius relation:

$$\frac{dn_U}{dt} = -k_1 n_U \tag{2.6}$$

where n_U is a molar quantity of urea.

It takes time for isocyanic acid to evaporate from the molten mixture since it does not have large vapor pressure. The effusion equation is used to describe the evaporation of isocyanic acid. The temperature dependency of the vapor pressure of pure isocyanic acid is estimated with the Clausius-Clapeyron equation with the heat of vaporization $\Delta_{lg}H_{HNCO} = 20.6\ \mathrm{kJ/mol}$ at the boiling point 23.5℃. Since isocyanic acid is resolved in the molten mixture, the Henry's law is applied to obtain the partial vapor pressure. With a proportional constant B irrelevant to temperature and a surface area A for evaporation, the evaporation equation and its kinetic relation of isocyanic acid are as follows:

$$\mathrm{HNCO\ (l)} \rightarrow \mathrm{HNCO\ (g)} \tag{2.7}$$

$$\frac{dn_{I,e}}{dt} = -A\beta\frac{n_I}{n_T} \tag{2.8}$$

where n_I is a molar quantity of isocyanic acid and the subscript e represents evaporation, and the kinetic constant β is defined as:

$$\beta = \frac{B}{\sqrt{T}}\exp\left[-\frac{\Delta_{lg}H_{HNCO}}{RT}\right] \tag{2.9}$$

Part of dissolved isocyanic acid reacts with biuret to form cyanuric acid with the chemical reaction:

$$\mathrm{C_2H_5N_3O_2\ (Biuret)\,(m) + HNCO\,(l) \rightarrow CYA\,(l) + NH_3\,(g)} \tag{2.10}$$

The ammonia in this reaction is also assumed to evaporate immediately from the solution as well. The chemical kinetics for the reaction of Eq. (2.10) is assumed a second-order with the kinetic constant $k_3 = A_3 \exp[-E_{a3}/RT]$:

$$\frac{1}{n_T}\frac{dn_B}{dt} = -k_3 \frac{n_I}{n_T}\frac{n_B}{n_T} \tag{2.11}$$

where n_T represents the total number of moles in the molten solution.

Lastly, biuret is formed as a result of the reaction between urea and isocyanic acid, which is reversible (Brack *et al.* (2014)):

Urea (m) + HNCO (l) → Biuret (m) (2.12)

The reaction of biuret formation is assumed fast in the molten solution. Isocyanic acid is added to the reaction of Eq. (2.12) by the decomposition of urea of Eq. (2.5) and biuret is removed by the reaction of Eq. (10). Since urea can be regarded as a solvent, it does not need to be included in the equilibrium constant that is written as [Biuret]/[HNCO]. Adding isocyanic acid and removing biuret make the equilibrium constant smaller, so they act as driving forces for the forward reaction of Eq. (2.12) by le Chatelier's principle. Those driving forces lead to the assumption that the chemical kinetics for forward reaction will be relatively fast. Since the forward reaction of Eq. (2.12) is dominant during the pyrolysis of urea, the reaction of Eq. (2.12) is assumed to reach the equilibrium in no time.

2.4 Two-Step approach

The urea pyrolysis is modeled consisting of the kinetic time-marching and equilibrium correction steps with in-between evaporation of ammonia and isocyanic acid to describe its chemical reactions. Combining the kinetic and equilibrium steps, molar quantities in the solution are updated as:

$$n_U(t+\delta t) = n_U(t) + \delta n_U - \Delta \tag{2.13}$$

$$n_I(t+\delta t) = n_I(t) + \delta n_I - \Delta \tag{2.14}$$

$$n_B(t+\delta t) = n_B(t) + \delta n_B + \Delta \tag{2.15}$$

$$n_C(t+\delta t) = n_C(t) + \delta n_C \tag{2.16}$$

The molar increment δn and correction factor Δ are determined in the kinetic step and equilibrium correction step respectively and they will be described below. The correction factor Δ does not have influence on cyauric acid because the factor comes from the reaction of biuret formation (2.12).

The kinetic step accounts for the reactions (2.5), (2.7), and (2.10) where the time increment δt is involved. The kinetic equations of urea pyrolysis are expressed in terms of molar increment of each species. Urea decomposition Eq. (2.6) and cyanuric acid formation (2.11) are rewritten by the explicit Euler scheme:

$$\frac{\delta n_U}{n_T} = -k_1 \frac{n_U}{n_T} \delta t \tag{2.17}$$

$$\frac{\delta n_B}{n_T} = -k_3 \frac{n_I}{n_T} \frac{n_B}{n_T} \delta t \tag{2.18}$$

The change of isocyanic acid in the molten solution comes from urea

evaporation (2.9) besides the urea decomposition and cyanuric acid formation:

$$\frac{\delta n_I}{n_T} = \left[k_1 \frac{n_U}{n_T} - A\beta \frac{n_I}{n_T^2} - k_3 \frac{n_I}{n_T} \frac{n_B}{n_T} \right] \delta t \tag{2.19}$$

and the change of cyanuric acid is equal to the change of biuret:

$$\delta n_C = -\delta n_B \tag{2.20}$$

For the in-between evaporation, ammonia is formed by the reactions of urea decomposition and cyanuric acid formation and it leaves the mixture immediately:

$$\delta n_{A,e} = -\delta n_U - \delta n_B \tag{2.21}$$

Also part of isocyanic acid evaporates from the molten solution by the equation (2.8) rewritten as:

$$\delta n_{I,e} = A\beta \frac{n_I}{n_T} \delta t \tag{2.22}$$

Next step is to impose the effect of the reaction equilibrium. The biuret formation (2.12) is assumed to take no time to reach equilibrium. The equilibrium constant remains the same during pyrolysis with the total moles of the molten solution $n'_T = n_T + \sum_{sol'n} \delta n - \Delta$ and so it can be written as:

$$\frac{n_B / n_T}{n_U / n_T \times n_I / n_T} = \frac{\left(n_B + \delta n_B + \Delta\right) / n'_T}{\left(n_U + \delta n_U - \Delta\right) / n'_T \times \left(n_I + \delta n_I - \Delta\right) / n'_T} \tag{2.23}$$

Then Δ can be obtained by the linearized equation:

$$\Delta\left(\frac{1}{n_B}+\frac{1}{n_U}+\frac{1}{n_I}-\frac{1}{n_T}\right)+\left(\frac{\delta n_B}{n_B}+\frac{1}{n_T}\sum_{sol'n}\delta n-\frac{\delta n_U}{n_U}-\frac{\delta n_I}{n_I}\right)=0 \tag{2.24}$$

A single time step finishes by collecting the molar increments δn and correction factor Δ and updating molar quantities of each species by the equations from (2.13) to (2.16). In this way, the reactions for pyrolysis can proceed to a target time if model parameters are known. Next section will deal with a topic of kinetic parameters, which will be determined by experiment.

2.5 Governing equations of urea pyrolysis

Though time integration can be done with two-step approach discussed in the previous section, it is not easy to analyze the error of the numerical scheme since the evaporation and equilibrium equations are involved in the time march. Higher order integration schemes for ordinary differential equations are also difficult to apply. Therefore governing equations are built with sourcing the equilibrium correction from biuret formation in this section.

Equations (2.13) through (2.15) combining the kinetic and equilibrium equations become a set of ordinary differential equations as the time increment is set infinitesimal. For example, the right hand side of Eq. (2.13) is Taylor-expanded with Eq. (2.17) as:

$$n_U(t+\delta t)\approx n_U(t)+\frac{dn_U}{dt}\delta t=n_U(t)-k_1 n_U\delta t-f_\Delta\delta t \tag{2.25}$$

where $\Delta = f_\Delta \delta t$ and f_Δ is defined from Eq. (2.24) as:

$$f_\Delta = -\frac{\begin{array}{c}\left(\frac{1}{n_T}-\frac{1}{n_U}\right)\left(-k_1 n_U\right)+\left(\frac{1}{n_B}\right)\left(-k_3\frac{n_I n_B}{n_T}\right) \\ +\left(\frac{1}{n_T}-\frac{1}{n_I}\right)\left[k_1 n_U - A\beta\frac{n_I}{n_T}-k_3\frac{n_I n_B}{n_T}\right]\end{array}}{\frac{1}{n_B}+\frac{1}{n_U}+\frac{1}{n_I}-\frac{1}{n_T}} \tag{2.26}$$

then the equations for the number of moles of urea, isocyanic acid, biuret and cyauric acid are expressed as:

$$\frac{dn_U}{dt} = -k_1 n_U - f_\Delta \tag{2.27}$$

$$\frac{dn_I}{dt} = k_1 n_U - A\beta\frac{n_I}{n_T} - k_3\frac{n_I n_B}{n_T} - f_\Delta \tag{2.28}$$

$$\frac{dn_B}{dt} = -k_3\frac{n_I n_B}{n_T} + f_\Delta \tag{2.29}$$

$$\frac{dn_C}{dt} = k_3\frac{n_I n_B}{n_T} \tag{2.30}$$

The evaporating amount of ammonia and isocyanic acid is calculated using Eqs. (2.21) and (2.22) as:

$$\frac{dn_{A,e}}{dt} = k_1 n_U + k_3\frac{n_I n_B}{n_T} \tag{2.31}$$

$$\frac{dn_{I,e}}{dt} = A\beta\frac{n_I}{n_T} \tag{2.32}$$

Equations (2.27) through (2.32) are a system of ordinary differential equations and can be solved by an ordinary differential

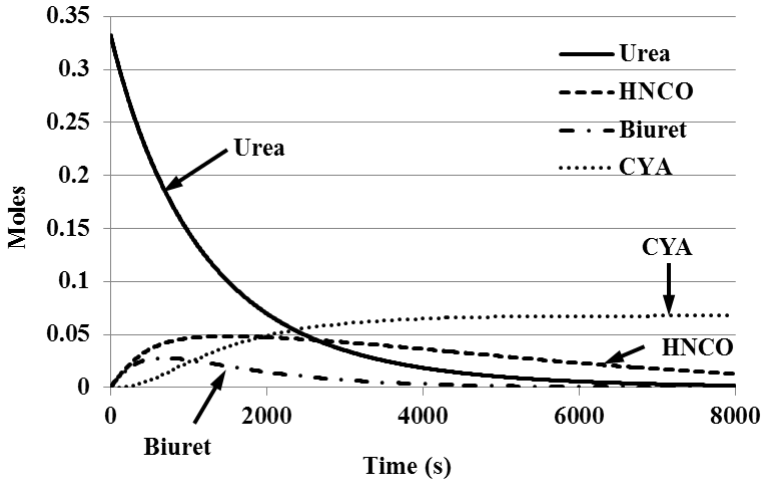

Figure 2.3 Molar history in the solution: Reactor area 0.154 m^2 at the temperature 200℃, initial urea mass 20 g

equation solver. It is noted that f_Δ is singular when $n_I = 0$ or $n_B = 0$. At least small traces of isocyanic acid and biuret are physically expected to exist in the solution. Therefore small quantities need to be put as the initial conditions for isocyanic acid and biuret.

A solver code for the ordinary differential equations for urea pyrolysis is listing in Appendix B.2. The governing equations are solved by the Octave 3.6.1 lsode routine. The core source Eqs. (2.26) to (2.32) is implemented as shown in Code 2.1:

Code 2.1 Implementation of the governing equations

```
fdel=(1/nt-1/nu)*(-k1*nu)+1/nb*(-k3*ni*nb/nt);
fdel=fdel+(1/nt-1/ni)*(k1*nu-Ae*be*ni/nt-k3*ni*nb/nt);
fdel=-fdel/(1/nb+1/nu+1/ni-1/nt);
ndot(1)=-k1*nu-fdel;
ndot(2)=k1*nu-Ae*be*ni/nt-k3*ni*nb/nt-fdel;
ndot(3)=-k3*ni*nb/nt+fdel;
ndot(4)=k3*ni*nb/nt;
ndot(5)=k1*nu+k3*ni*nb/nt;
ndot(6)=Ae*be*ni/nt;
```

The detailed implementation of urea pyrolysis is consulted in Appendix B.2. The parameters for chemical kinetics used in the code are explained in next section. The pyrolysis simulation is for a reactor with evaporating area 0.154 m^2 at 200℃ and a urea sample of 20 g. At the initial stage urea decomposition supplies isocyanic acid and they form biuret in Fig. 2.3. It takes some delay to form cyauric acid. Evaporating species of ammonia and isocyanic acid are also calculated by Eqs. (2.31) and (2.32). Figure 2.4 shows the accumulated molecules that evaporate to the surrounding gas. Figure 2.5 shows the solution and evaporated mass. Urea decomposition will be discussed in later section in detail.

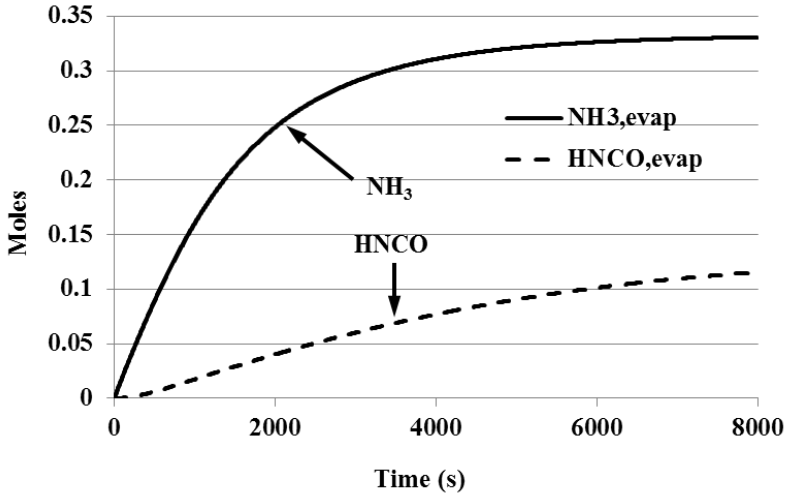

Figure 2.4 Cumulating plot of evaporated species: Reactor area 0.154 m^2 at the temperature 200℃, initial urea mass 20 g

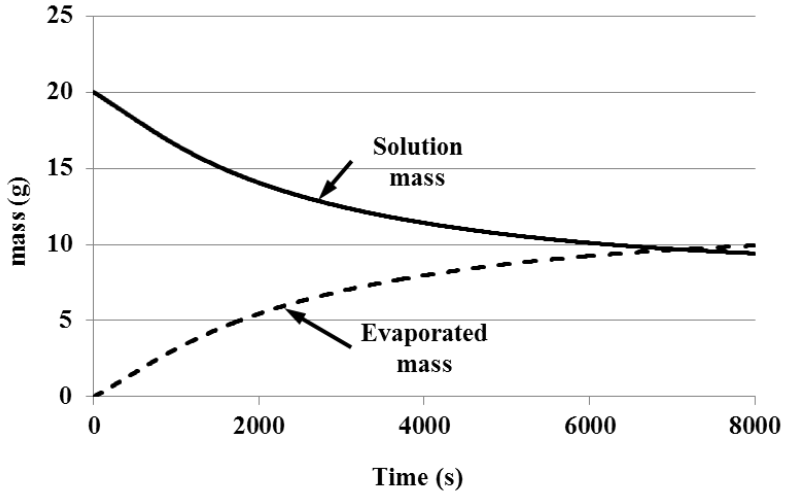

Figure 2.5 Solution and evaporated Mass history: Reactor area 0.154 m^2 at the temperature 200℃, initial urea mass 20 g

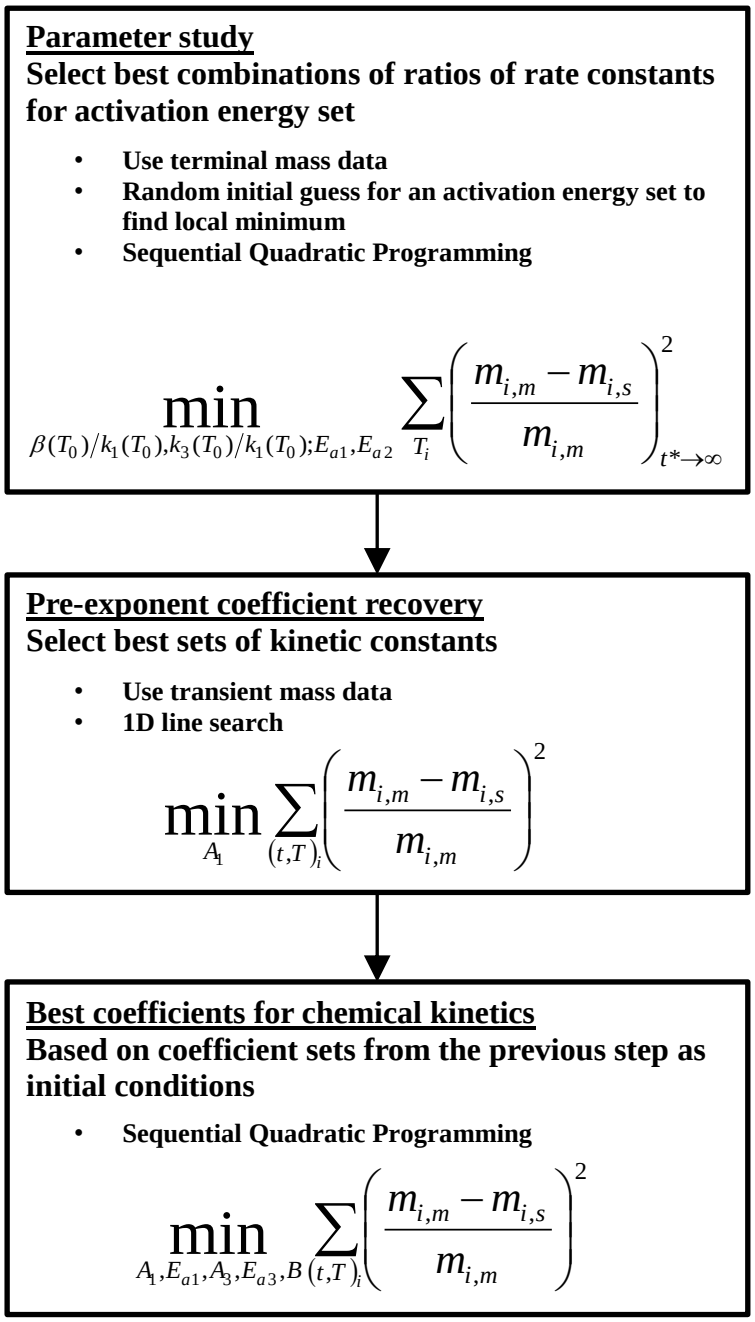

Figure 2.6 Flow chart of determining kinetic constants for the chemical reaction and evaporation model

2.6 Determination of kinetic parameters

There are unknown five constants in the pyrolysis model: pre-exponential factors A_1, A_3, B and Arrhenius activation energies E_{a1}, E_{a3}. Those constants are determined by measuring masses at different temperatures. Though there are mass data available from experiment, it is not easy to determine those constants all at once when a general optimization scheme is applied because the pre-exponential factors and the activation energies are of different order of influence on the objective. It causes that less influential constants on the system can be easily stuck around a local value during optimization. So the influence-scale problem is handled by grouping constants: pre-exponential factors will be determined after activation energies are obtained.

The model is a highly nonlinear system so that it is not easy to obtain best-fit parameters by minimizing an objective function of the relative error between measurement and calculation. It should be provided with proper initial values for optimization. Flow chart for determination of the five constants is shown in Fig. 2.6. First two steps are used to generate good initial conditions for optimization. First step determines ratios of rate constants with parameter study on activations energy. With the best 100 candidates from the first step, the best 10 candidates are selected from the second step by getting pre-exponential factors. Finally, it is good to go optimization based on those initial conditions to have the best-fit model constants. In this section, the way of obtaining model constants is described step-by-step.

To eliminate dependency on pre-exponential factors, terminal measured data are used with an introduction of scaled time. If a scaled time is defined as $t^* = t \times k_1(T)$, the governing equations from Eq. (2.27) to Eq. (2.30) can be written as:

$$\frac{dn_U}{dt^*} = -n_U - f_\Delta^* \tag{2.27}$$

$$\frac{dn_I}{dt^*} = n_U - A\frac{\beta}{k_1}\frac{n_I}{n_T} - \frac{k_3}{k_1}\frac{n_I n_B}{n_T} - f_\Delta^* \tag{2.28}$$

$$\frac{dn_B}{dt^*} = -\frac{k_3}{k_1}\frac{n_I n_B}{n_T} + f_\Delta^* \tag{2.29}$$

$$\frac{dn_C}{dt} = \frac{k_3}{k_1}\frac{n_I n_B}{n_T} \tag{2.30}$$

and the equilibrium sourcing term f_Δ^* of Eq. (2.26) turns as:

$$f_\Delta^* = -\frac{\left(\frac{1}{n_T}-\frac{1}{n_U}\right)(-n_U)+\left(\frac{1}{n_B}\right)\left(-\frac{k_3}{k_1}\frac{n_I n_B}{n_T}\right) + \left(\frac{1}{n_T}-\frac{1}{n_I}\right)\left[n_U - A\frac{\beta}{k_1}\frac{n_I}{n_T} - \frac{k_3}{k_1}\frac{n_I n_B}{n_T}\right]}{\frac{1}{n_B}+\frac{1}{n_U}+\frac{1}{n_I}-\frac{1}{n_T}}$$

One of benefits of the scaled time is that time range can be normalized so that it is less sensitive for change of parameters. It is important because proper terminal time is not known at that stage of fitting calculations with measured data. More importantly, dependency on pre-exponential constants can be suppressed.

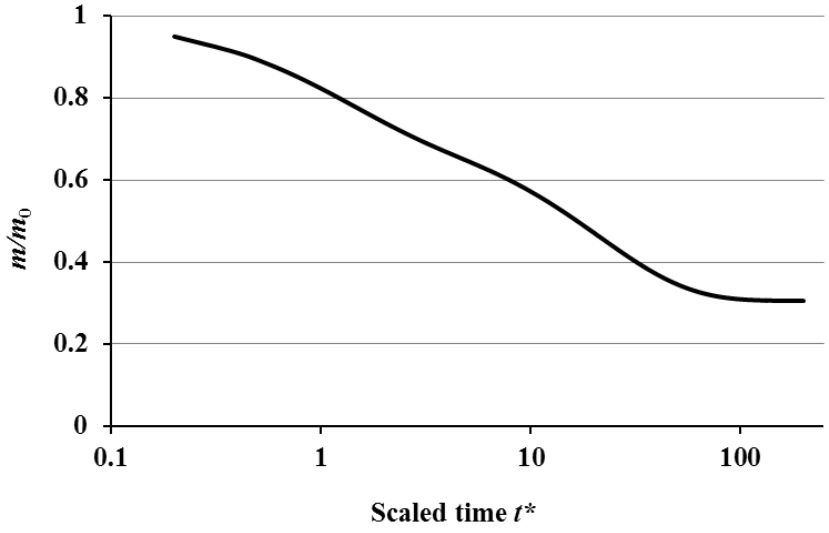

Figure 2.7 Simulation result of the mass residue of urea solution in the reactor with respect to the scaled time t^*. Initial urea mass is 20 g in a 70 mm diameter beaker

With those equations, the residue from urea pyrolysis can be obtained as time goes infinity $t^* \to \infty$. Figure 2.7 shows a simulation result of urea pyrolysis that the total mass converges on a terminal value. Candidates of the activation energies are obtained by finding ratios $\beta(T_0)/k_1(T_0)$ and $k_3(T_0)/k_1(T_0)$ such that the ratios minimize the sum of squared mass error:

$$\min_{\beta(T_0)/k_1(T_0),k_3(T_0)/k_1(T_0);E_{a1},E_{a2}} \sum_{T_i} \left(\frac{m_{i,m} - m_{i,s}}{m_{i,m}} \right)^2_{t^* \to \infty} \tag{2.36}$$

where T_0=180℃ and $T_i \in$(170℃, 180℃, 190℃, 200℃). Once the ratios at T_0 are guessed, the ratios at other temperatures are calculated with the relations in whom the pre-exponential factors are eliminated:

$$\frac{k_3(T)/k_1(T)}{k_3(T_0)/k_1(T_0)} = \exp\left[-\frac{E_{a3}-E_{a1}}{R}\left(\frac{1}{T}-\frac{1}{T_0}\right)\right] \tag{2.37}$$

$$\frac{\beta(T)/k_1(T)}{\beta(T_0)/k_1(T_0)} = \sqrt{\frac{T_0}{T}}\exp\left[-\frac{\Delta_{\lg}H_{\mathrm{HNCO}}-E_{a1}}{R}\left(\frac{1}{T}-\frac{1}{T_0}\right)\right] \tag{2.38}$$

Those ratios of ratios are used to get residue masses at different temperatures.

Parameter study is conducted for the activation energies. E_{a1} is discretized in the range from 55 to 95 kJ/mol by increment 5 kJ/mol. E_{a2} is examined in the range 105 to 195 kJ/mol by increment 5 kJ/mol. To avoid local minimum and get as global minimum as possible, initial state variables for $\beta(T_0)/k_1(T_0)$ and $k_3(T_0)/k_1(T_0)$ are randomly generated. Optimizations are performed several times by SQP algorithm shipped with OCTAVE code with the initial conditions. Simulations were done with a time step $\Delta t^* = 0.1$ and finished at $t_\infty^* \approx 100$. The initial conditions for species were set n_{Urea}=0.3321 mol and n_{HNCO}= n_{Biuret} =5.047x10^{-4} mol. In this first step, about 100 candidates are obtained for next step. It is noted that the terminal mass data are not close to ultimate residue of cyauric acid as shown in Fig. 2.8 since it takes very long time to finish the reactions. It should be also mentioned that there forms cyauric acid matrix that loses liquidity so that liquid mixture assumption fails. Despite these phenomena, the trend of residue is assumed to hold good.

The second step of guessing initial conditions is to find the pre-exponent constant A_1. Among the candidates of $\beta(T_0)/k_1(T_0)$ and $k_3(T_0)/k_1(T_0)$ corresponding to (E_{a1}, E_{a3}), one can find the best fit to the measured mass history of urea pyrolysis by one dimensional line search. With a fixed activation energy set (E_{a1}, E_{a3}), A_3 and B can

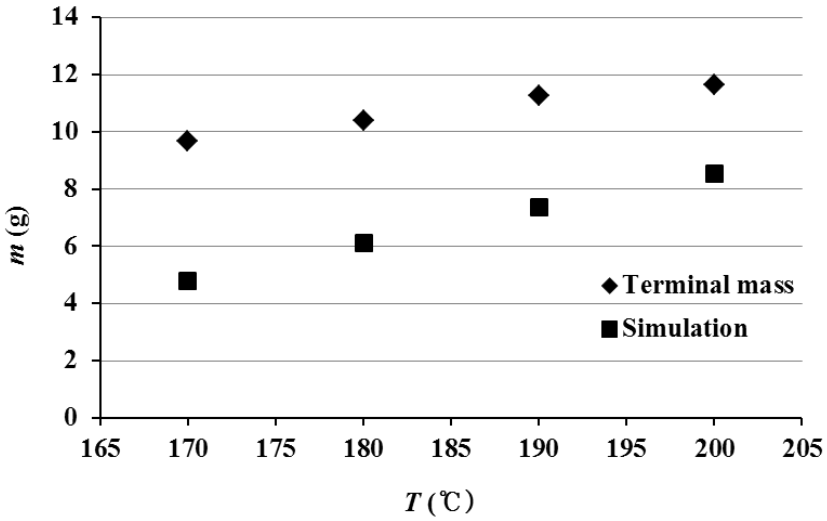

Figure 2.8 Residue masses from the scaled model and measured terminal masses. The initial mass of urea is 20 g in a 70 mm−diameter beaker.

expressed in terms of A_1 with the rate constant ratios $\beta(T_0)/k_1(T_0)$ and $k_3(T_0)/k_1(T_0)$ by:

$$A_3 = A_1 \exp\left[-\frac{E_{a1}-E_{a3}}{RT_0}\right]\frac{k_3(T_0)}{k_1(T_0)} \tag{2.39}$$

$$B = A_1\sqrt{T_0}\exp\left[-\frac{E_{a1}-\Delta H}{RT_0}\right]\frac{\beta(T_0)}{k_1(T_0)} \tag{2.40}$$

Equations (2.39) and (2.40) transform a fitting parameter problem into one dimensional optimization problem with single state variable A_1. The problem is defined as follows since the transient mass data are used in this step.

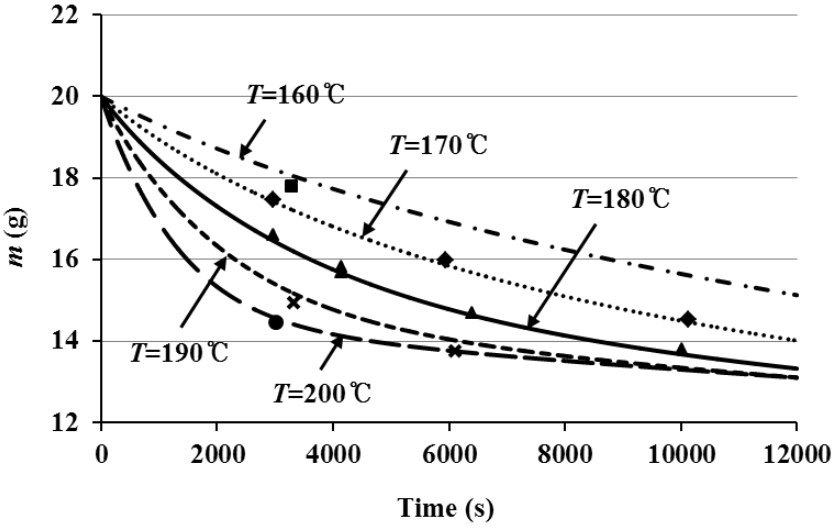

Figure 2.9 Measured and simulation results of the history of urea pyrolysis. The initial mass of urea is 20 g in a 70 mm-diameter beaker and each data point is obtained from a sample of an independent experiment.

$$\min_{A_1} \sum_{(t,T)_i} \left(\frac{m_{i,m} - m_{i,s}}{m_{i,m}} \right)^2 \tag{2.41}$$

Equation (2.41) is solved by the fminbnd routine in OCTAVE. As did in the parameter study of the first step, the best optimal values of Eq. (2.41) are selected since the activation energies are yet to be determined. They have been discretized so that they are just close to the optimal values. Therefore the final optimization has to be conducted with initial guesses from Eq. (2.41).

Although the system is highly non-linear, algorithms of non-linear programming can give best-fit parameters with initial conditions obtained through the previous steps since they are close to optimal state values. This is the final optimization problem with all parameters:

Confidence interval analysis
Based on coefficient sets as initial conditions

- **Student's t-test**
- **1D line search for each constants c_i and experimental data j**

$$\min_{c_i}\left(\frac{m_{j,m}-m_{j,s}}{m_{j,m}}\right)^2$$

Figure 2.10 Optimization definition for confidence interval analysis

$$\min_{A_1,E_{a1}A_2,E_{a2},B}\sum_{(t,T)_i}\left(\frac{m_{i,m}-m_{i,s}}{m_{i,m}}\right)^2 \tag{2.42}$$

where $(t,T)_i$ is the ith transient sample. Measured samples are listed Table 2.1 and shown in Fig. 2.9. Equation (2.42) is solved by the sqp routine in OCTAVE software. There are two final candidates which give a similar value of the objective function in table 2.2.

Regression by optimization to determine the best kinetic constants is not more effective since two sets gives the same objective value within tolerance. Confidence interval problem is devised to select one best-fit set assuming that physically probable set of kinetic constants has narrow confidence interval. It should be noted that the regression problem is highly non-linear; another optimization problem is defined for regression analysis as shown in Fig. 2.10.

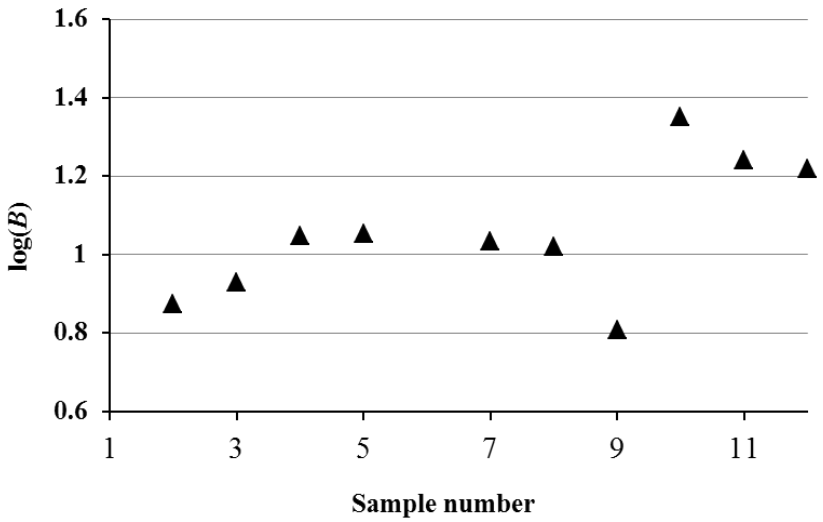

Figure 2.11 Kinetic constant B to recover sample data. Outliners for sample 1 and 6 are omitted in the plot.

$$\min_{c_i}\left(\frac{m_{j,m}-m_{j,s}}{m_{j,m}}\right)^2 \tag{2.43}$$

which is solved by the fminbnd routine in OCTAVE. A kinetic constant is recovered around the best-fit parameter to generate the target measured data. Equation (2.43) is solved for each kinetic constant and all measured data. Although the algorithm of one dimensional line search by the fminbnd routine is quite robust, some measured data cannot be obtained by Eq. (2.43). In that case, the data are dropped since they can be considered outliers. Figure 2.11, for example, shows the kinetic constant B to match measured data. Sample number 1 and 6 cannot be recovered from Eq. (2.43) so that they are omitted from the plot. The other pre-exponent constants are also treated with logarithmic value to match the influence of activation energies on the system since activation energies are in the log function. Student-t

test by R software is conducted for obtaining confidence interval and the results are in Table 2.2. Confidence interval of case 69 is broader than that of case 52. Therefore it is concluded that the kinetic parameters from case 52 explains the experimental data well and the parameters from case 69 are dismissed.

Figures 2.9 show measured and best-fit simulation results of the residual mass and the history of urea pyrolysis. The parameters of the pyrolysis model obtained by the simulation and measurement are listed in Table 2.3.

Table 2.2 Best-fit kinetic constants to recover measured mass and their confidence interval

Case	#52		#69	
Kinetic constants	Value	95% Confidence interval	Value	95% Confidence interval
A_1 s	2.502×10^{5}	$(2.375\times10^{5}, 2.794\times10^{5})$	1.987×10^{6}	$(1.88\times10^{6}, 2.03\times10^{6})$
E_{a1} kJ/mol	76.92	(76.5,77.1)	84.45	(84.1,84.7)
A_3 s	2.702×10^{13}	$(1.23\times10^{13}, 2.77\times10^{14})$	7.001×10^{17}	$(1.88\times10^{16}, 1.07\times10^{21})$
E_{a3} kJ/mol	143.4	(134,147)	184.6	(170,220)
B mol/m^{2}sK$^{0.5}$	11.99	(7.23,14.5)	11.08	(7.86,18.8)

Table 2.3 Kinetic reactions and models used to describe urea pyrolysis: Five parameters A_1, E_{a1}, A_3, E_{a3}, and B were set to best fit to measurement

Reaction	Kinetic constant
Urea(m)→HNCO(l)+NH_3(g) $\frac{dn_U}{dt} = -k_1 n_U$	$k_1 = A_1 \exp\left[-\frac{E_{a1}}{RT}\right]$ where, $A_1 = 2.502\times10^5 / \mathrm{s}$ $E_{a1} = 76.92\ \mathrm{kJ/mol}$
Biuret(m)+HNCO(l)→ CYA(s)+NH_3(g) $\frac{1}{n_T}\frac{dn_B}{dt} = -k_3 \frac{n_I}{n_T}\frac{n_B}{n_T}$	$k_3 = A_3 \exp\left[-\frac{E_{a3}}{RT}\right]$ where, $A_3 = 2.702\times10^{13}/\mathrm{s}$ $E_{a3} = 143.6\ \mathrm{kJ/mol}$
HNCO(l)→HNCO(g) $\dot{n}''_{I,e} = -\beta \frac{n_I}{n_T}$	$\beta = \frac{B}{\sqrt{T}} \exp\left[-\frac{\Delta_{\lg} H_{\mathrm{HNCO}}}{RT}\right]$ where, $B = 11.99\ \mathrm{mol/m^2 sK^{0.5}}$ $\Delta_{\lg} H_{\mathrm{HNCO}} = 20.6\ \mathrm{kJ/mol}$

Table 2.4 Comparison of the kinetics of urea decomposition. D_d is the diameter of a urea droplet and c_U is the molar concentration of urea with $[c_U]$=mol/ml

Model	Authors	Constant
$\dot{n}_U = -A\exp\left[-\frac{E_a}{RT}\right]n_U$	Yim et al. (2004)	$A = 4.855\times10^3/\mathrm{s}$ $E_a = 23\ \mathrm{kJ/mol}$
	Aoki et al. (1999)	$A = 1.268\times10^4/\mathrm{s}$ $E_a = 65\ \mathrm{kJ/mol}$
	Present study	$A_1 = 2.502\times10^5\ /\mathrm{s}$ $E_{a1} = 76.92\ \mathrm{kJ/mol}$
$\dot{c}_U = -A\exp\left[-\frac{E_a}{RT}\right]c_U^{0.3}$	Brack et al. (2014)	$A = 2.0\times10^4$ $\mathrm{mol}^{0.7}/\mathrm{ml}^{0.7}\mathrm{s}$ $E_a = 74\ \mathrm{kJ/mol}$
$\dot{m}_U = -\pi D_d A\exp\left[-\frac{E_a}{RT}\right]$	Birkhold et al. (2007)	$A = 0.42\ \mathrm{kg/m\cdot s}$ $E_a = 69\ \mathrm{kJ/mol}$

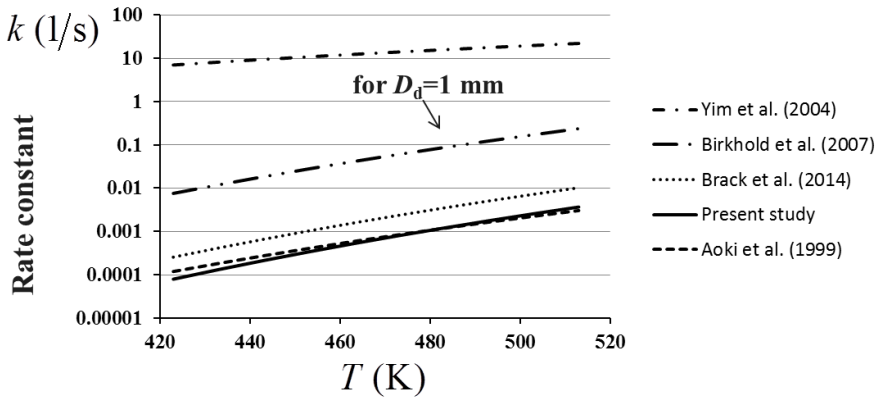

Figure 2.12 Comparison of the rate constant for urea decomposition $\dot{n}_U / n_U$

2.7 Model validation of urea pyrolysis

The validity of the proposed urea pyrolysis model is examined by comparing its prediction on urea pyrolysis to those of other authors. Table 2.4 presents the pre-exponential factors and activation energies of the models. Yim *et al.* (2004), Aoki *et al.* (1999) and the present model assume a first-order reaction for urea pyrolysis. Yim *et al.* (2004) anticipated the fastest decomposition of urea among the models as shown in Fig. 2.12. There is an argument on the activation energy that they calculated since they conducted the experiments in the aluminum tubular reactor where it is possible for HNCO hydrolysis to disturb and reduce the activation energy of urea pyrolysis (Zonoelo, E.F. 2009). Aoki *et al.* (1999) gave the same rate constant as that of the present model in temperature range of the present experiment. Brack *et al.* (2014) proposed a fractional order of urea pyrolysis with the molar concentration of urea in the mixture.

Figure 2.12 shows the rate constant $k = A\exp\left[-E_a/RT\right]$ of the models in Table 2.4 while for the model of Brack *et al.* (2014) the initial decomposition rate $-\dot{n}_U / n_U = A\exp\left[-E_a/RT\right]c_U^{0.3} V_R / n_U$ is

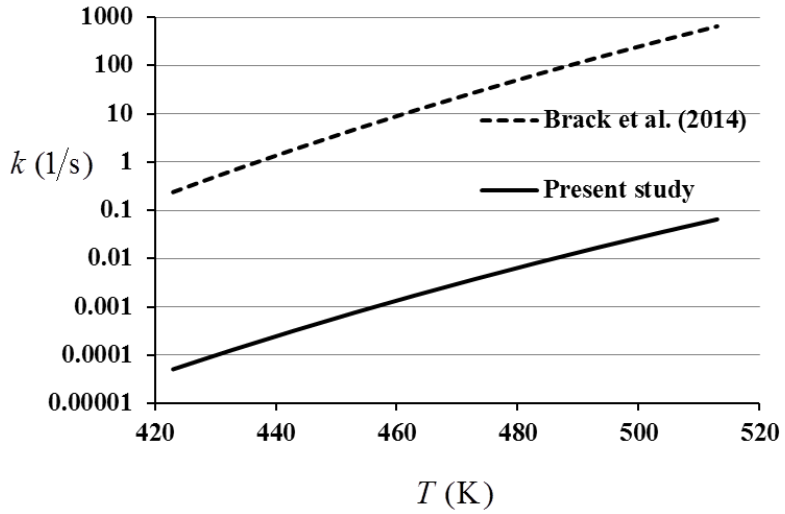

Figure 2.23 Rate constant comparison for cyauric acid formation

plotted with an assumption on liquid urea density of 1.3 g/cm^3. V_R is the volume of the mixture. Birkhold *et al.* (2007) suggested a model applicable to a urea droplet of which the form is taken from the models of saturated droplet evaporation. The rate constant of Birkhold *et al.* (2007) in Fig. 2.12 is obtained by dividing the model by urea mass as:

$$-\dot{m}_U / m_U = \pi D_d / m_U \, A \exp\left[-E_a / RT\right] \tag{2.45}$$

It is worth noting that the model is not intensive for one species decomposition since the right hand size of Eq. (2.45) is inversely proportional to $m_U^{2/3}$. It is not physically reasonable that intensive decomposition rate is dependent on the current amount of mass as shown in Fig. 2.12.

The urea decomposition of Yim et al. (2004) and Brack et al.

(2014) is faster than that of Aoki et al. and the current study. As mentioned earlier, it is reported that aluminum seems to reduce the activation energy of urea related species. Table 2.5 tells that Brack et al. (2014) also used aluminum containing crucible as their reactor. Yim et al. (2004) filled glass beads in the aluminum tube to increase residence time and Brack et al. used an alumina crucible of small diameter. Their reactors gives chance to react with reactor wall so that the materials affect the reactions.

Figure 2.13 shows that the rate constant k_3 for cyauric acid of Brack et al. (2014) is much higher than that of the present study. Brack et al. (2014) use chemical reaction model of $\dot{n}_C = kV_R c_B c_I$ and the rate constant is converted to be the equivalent constant as $k_3 = k\, n_T / V_R$. It is worth nothing that triuret take part in the reaction of cyanuric formation over 200℃. Therefore it should be added the following reactions for such condition (Brack et al. (2014)).

$$\text{biuret(m)} + \text{HNCO(g)} \rightarrow \text{triuret(s)} \tag{2.46}$$

$$\text{triuret(s)} \rightarrow \text{CYA(s)} + \text{NH}_3\text{(g)} \tag{2.47}$$

Triuret explains more the amount production of cyanuric acid at higher temperature.

Table 2.5 Comparison of experimental setup for urea decomposition

	Present study	**Aoki et al. (1999)**	**Yim et al. (2004)**	**Brack et al. (2014)**
Reactor type	**Open reactor**	**Flow reactor**	**Flow reactor**	**Open reactor**
Reactor material	**Glass beaker**	**Ceramic tube**	**Aluminum tube**	**Alumina crucible**
Reactor dimension	***D*=70 mm**	***L*=50 cm**	***D*=0.75 cm** ***L*=7 cm**	***D*=4.3 mm**
T	**433-473 K**	**1083-1383 K**	**423-723 K**	**423-673 K**
***T* control**	**Constant**	**Constant**	**Constant**	**Sweep (TGA: 2-10 K/min)**
Note			**Aluminum reduces activation energy for urea related products (Zanoelo, E.F. (2009))**	

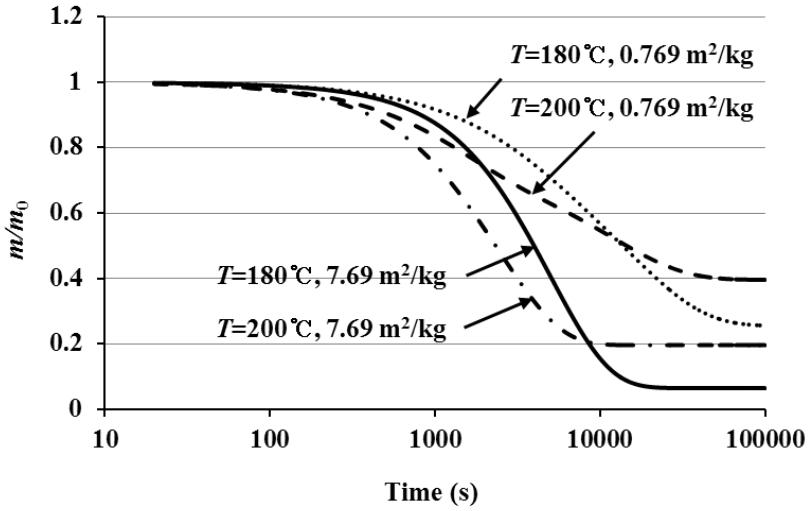

Figure 2.24 Influence of specific surface area and temperature on urea decomposition

2.8 Temperature and area to mass ratio

While the chemical reactions of the model is volumetric, isocyanic acid volumetrically takes part in the reactions. However the evaporation of isocyanic acid depends on the available surface area. When the urea film forms on the wall, the depth and specific surface area are related with the relation $Area/mass = 1/\rho h$. Figure 2.24 shows the influences of temperature and specific surface area on urea decomposition. The specific surface areas 7.69 m^2/kg and 0.769 m^2/kg are equivalent to initial depth of 0.1 mm and 1 mm of liquid urea on infinite plane, respectively.

The amount of cyanuric acid left on the reactor is determined as a result of rate competition between the formation of cyanuric acid and the evaporation of isocyanic acid. The temperature and the specific area are main factors affecting the rates respectively. The quantity of cyauric acid left on the wall is the greatest when the wall temperature is 200℃ and the initial depth of urea is 1 mm. The byproduct

deposition from urea decomposition is larger due to high yield of cyanuric acid at high temperature as experimentally confirmed in Fig. 2.8. The deposition quantity increases as the specific surface area is smaller since the residence time of isocyanic acid in the mixture is longer. Isocyanic acid remains so long as shown in Fig. 2.27 compared to Fig. 2.25 that it can supply with an ingredient to cyanuric formation for a long time. Figures 2.26 and 2.28 show that the ammonia evaporation is not affected greatly by specific area as the model assumes the ammonia evaporates immediately when it is produced. On the other hand, the evaporation of isocyanic acid heavily depends on the area to mass ratio. Figures from 2.24 to 2.28 suggest that when the impingement of aqueous urea spray on the wall is inevitable, the specific surface area should be as large and the wall temperature as low as possible.

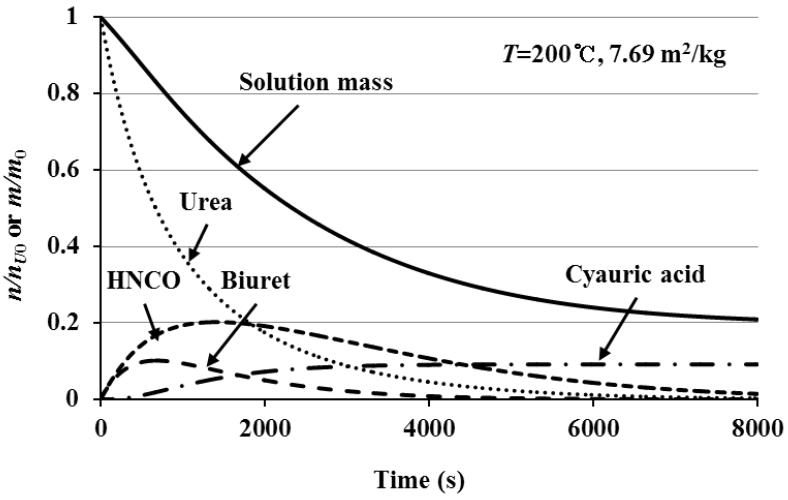

Figure 2.25 Simulation history of the amount of moles and mass in the reactor: T=200℃, A/m_0=7.69 m^2/kg

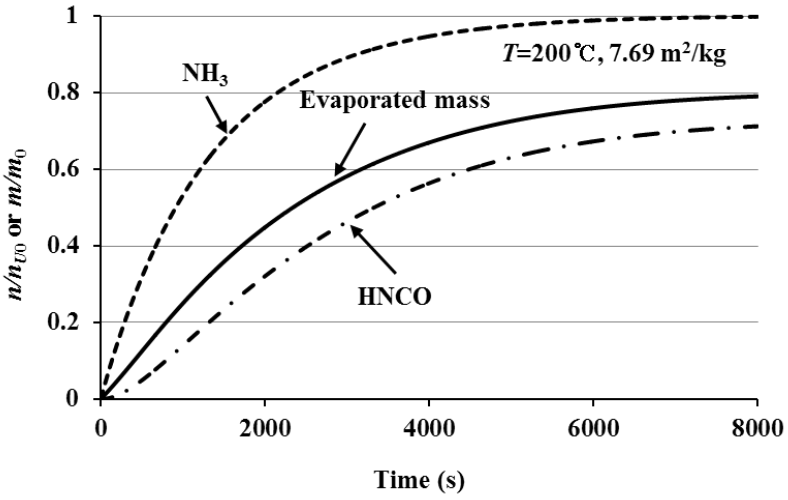

Figure 2.26 Simulation history of the cumulative amount of moles and mass that left the reactor: T=200℃, A/m_0=7.69 m^2/kg

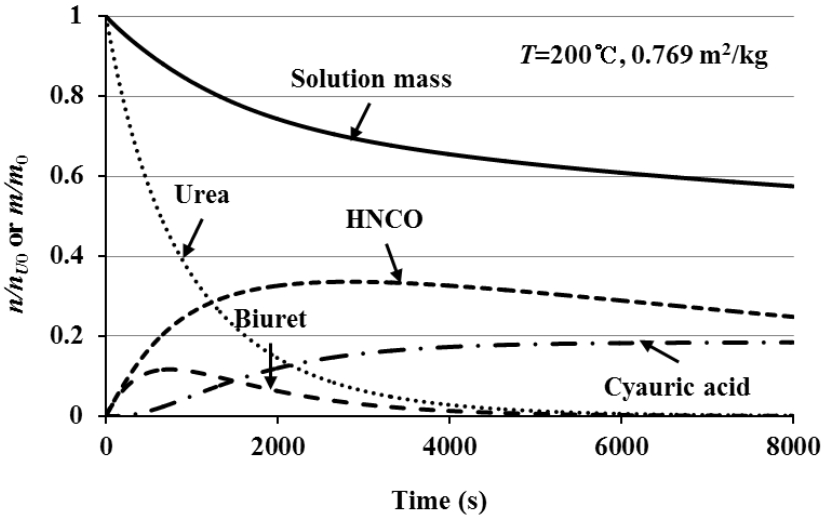

Figure 2.27 Simulation history of the amount of moles and mass in the reactor: T=200℃, A/m_0=0.769 m^2/kg

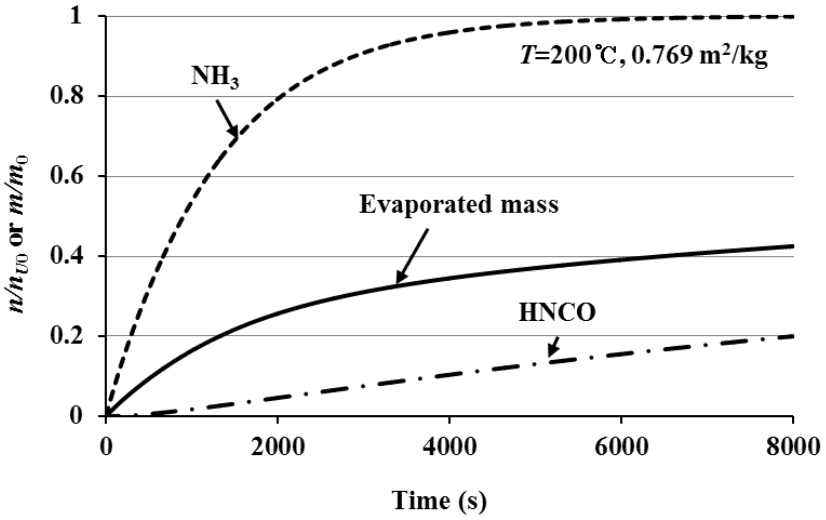

Figure 2.28 Simulation history of the cumulative amount of moles and mass that left the reactor: T=200℃, A/m_0=0.769 m^2/kg

2.9 Summary

A urea pyrolysis model for the temperature around 200℃ is developed to describe deposition on the surface of the SCR system. Five species are selected and the reactions among them are set to make a urea pyrolysis model. The chemical parameters are found by minimizing errors on mass between simulation and measurement. They are listed in Table 2.3. The results from the model are summarized as follows.

1) Production lag for cyauric acid: The proposed model anticipates that cyauric acid needs time to be produced or the chemical reaction for cyauric acid can be dropped for aqueous urea droplet applications since their interesting time period is so short to produce cyauric acid.

2) Competition between temperature and specific surface: Deposits form as reaction proceeds when a urea film is set on the surface. It is shown that the temperature and specific surface area are main factors to determine the amount of deposits. The terminal quantity of deposits, mainly cyanuric acid, increases at higher reaction temperature and deeper depth of the film.

Chapter 3
Water vaporization from aqueous urea

3.1 Introduction

Finely sprayed aqueous urea in a Urea-SCR system is injected into the exhaust gas stream. Since ammonia is used as a reducing agent in reducing NOx, urea has to be converted into ammonia. To recapitulate briefly, main desirable processes before the catalyst are divided into three steps: evaporation, pyrolysis, and hydrolysis. Water evaporates from aqueous urea drop in the urea decomposition process, which is followed by the pyrolysis and hydrolysis of urea to form ammonia and carbon dioxide in the gas phase, and then they are mixed with the products of combustion and fed on the SCR catalyst (Lundstrom *et al.* (2009); Wang *et al.* (2009)).

To predict the drop depletion of aqueous urea, water evaporation should be well modeled since the process gives initial conditions to the following decomposition of urea. One of the approaches to handle the water evaporation from aqueous urea is that the water evaporation is assumed to take place without considering the presence of urea (Lundstrom *et al.* (2009); Birkhold *et al.* (2006, 2007); Grout *et al.* (2013); Strom *et al.* (2009)). This approach makes it possible to use models of evaporation and heat transfer that have been successfully applied to fuel drops (Abramzon *et al.* (1989); Aggarwal *et al.* (1995); Sazhin, S.S.(2006)). The other approach is to reflect properties of aqueous urea as a binary mixture, which is the boiling-point change because of enrichment of urea as water evaporates. Sirignano and Wu (2008) suggested an effective boiling point from the Raoult's law, and Abu-Ramadan *et al.* (2011) applied it to the water evaporation from the aqueous urea. Ryddner and Trujillo (2015) used phase equilibrium

conditions for the urea and water driven from the Peng-Robinson equation to describe the depletion of a droplet.

The effective boiling point proposed by Sirignano and Wu (2008) needs to be verified for the application to the aqueous urea because the boiling-point elevation of the aqueous urea has not been confirmed experimentally so far to the best knowledge of authors. An equation which governs boiling-point elevation with respect to urea concentration in water is derived, which turns out to be equivalent to the effective boiling point, and it is verified by the boiling-point measurement as well. A water vaporization model is then proposed underlining the effect of the enthalpy of dissolution of urea in water, which has been ignored by previous works. The model is also supported by measurements. Finally, we apply the boiling-point elevation and the water vaporization models to the water evaporation from urea-water drop, and compare with the experiments of Wang *et al.* (2009) and Musa *et al.* (2006).

So far the CFD simulations have been mainly applied to design the channel for predicting ammonia production and mixing quality with combustion products at the catalyst inlet. The CFD practices sacrifices the accuracy of intermediate processes such as water evaporations and urea pyrolysis which is not of interest. It causes difficulty in predicting drop-wall interaction and wall precipitation where drop temperature and mole fractions of species need to be accurate.

To correctly evaluate the behavior of droplets, the properties for urea water solution should be examined. Since urea in the solution acts as a non-volatile solute, the thermo-physical properties of the mixture change according to relative mole fractions of each species. Those properties are called colligative properties that depend on the ratio of the number of solute particles to that of solvent molecules in a solution. Colligative properties include vapor pressure lowering,

boiling-point elevation, freezing-point depression, osmotic pressure and change in heat of vaporization. Though colligative properties are mostly studied for dilute solutions, urea-water solution used in Urea-SCR systems is not dilute. Initial fraction of urea in the solution is 32.5 wt. % or the molar urea fraction x_U is about 0.12. As water evaporates, the urea fraction increases since the urea is not volatile. Therefore, a model should be developed to describe a non-dilute system, which is one subject of this chapter.

The properties of boiling-point elevation and change in heat of vaporization of water are important to describe the evaporating behavior of water. Prior CFD practices ignore the colligative properties mainly due to lack of supporting experimental data. Even some researchers try to take the boiling-point elevation into a droplet analysis; they have not applied their model in full 3D CFD simulation.

In this chapter boiling-point elevation of urea water solution is measured and a model to describe the phenomenon is proposed. Heat transfer model is proposed as well reflecting the boiling-point elevation and change in heat of vaporization of water in the solution which is also a colligative property. Based on the revealed properties, water evaporation from aqueous droplets is analyzed under the natural convection with 1D simulation and the forces convection with 3D CFD simulation.

3.2 Experimental apparatus and measurement

Commercially available aqueous urea (Javanox^{TM}) is used, which is made especially for automotive applications without any further purification. Urea powder is prepared by evaporating water from the aqueous urea on a hot plate at 85° C in a glove box with ventilation.

Mixture samples for boiling tests as shown in Fig. 3.1 are

prepared by adding urea powder into a urea-water-solution of 32.5 wt. % of urea to meet the target concentration of urea. The samples are boiled in a 250 ml beaker with a 70 mm diameter over a gas burner. A k-type thermocouple is used to measure the temperature of samples. The boiling point is identified by intersecting two trend lines of sensible and latent heat regions as shown in Fig 3.2. Unlike pure water boiling, the temperature of boiling mixture increases with time due to water vaporization.

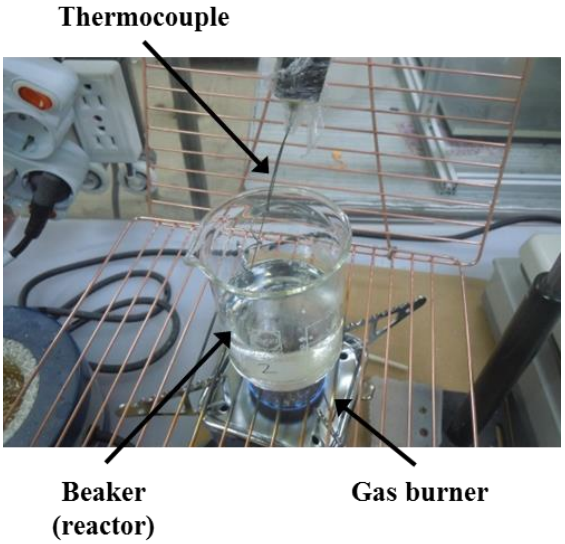

Figure 3.1 Experimental setup for boiling point elevation

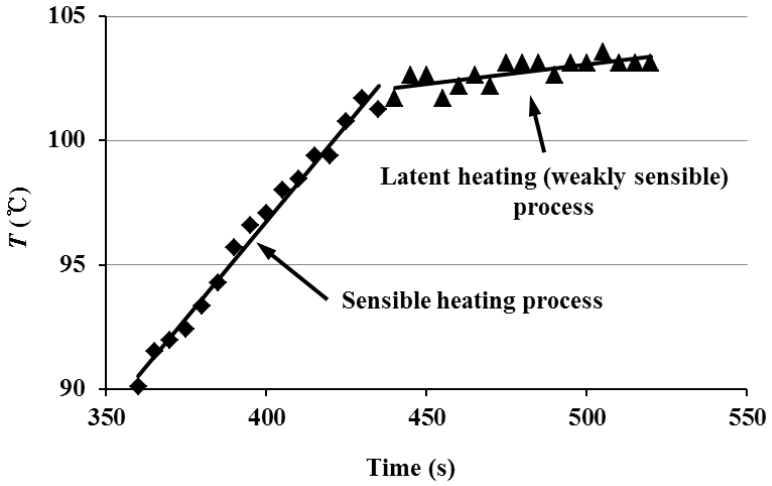

Figure 3.2 Boiling point measurement by intersecting the trend lines of sensible and latent heating regions

3.3 Boiling-point elevation

Commercial aqueous urea for vehicle applications has 32.5 wt. % of urea, and it is equivalent to the mole fraction of urea x_U=0.126. It is known that quite amount of urea can dissolve in water. For example, 400 g of urea dissolves in 100 ml of water without solidification, and the solubility increases further as temperature rises (Ryddner *et al.* (2015)). Urea can be considered a non-volatile solute in water, and does not give rise to solidification problem despite urea enrichment during water evaporation due to its high solubility at a high solution temperature.

When the urea concentration in water is high, the well-known model of the boiling-point elevation driven for a non-volatile solute in an ideally dilute solution is not applicable, which is given by

$$\Delta T_{b.p.} = \frac{RT_{n.b.p.}^2}{\Delta H} x_U \tag{3.1}$$

For the solution with high urea concentration, Eq. (3.1) should be modified. With ideal solution and gas assumptions, the free energy of water in solution can be described as

$$\mu_{W,l} = \mu^*_{W,l}(T) + RT \ln x_W \tag{3.2}$$

where the asterisk * indicates a pure substance and x_W is the mole fraction of water in the mixture. Under the ideal gas assumption, the free energy of water in gas phase is given by,

$$\mu^*_{W,g} = \mu^\circ_{W,g}(T) + RT \ln(P/P^\circ) \tag{3.3}$$

The equilibrium reaches when the free energy of water in the mixture becomes the same as that of water vapor as follows,

$$\mu_{W,l}(T+\Delta T,P)=\mu^{*}_{W,g}(T+\Delta T,P) \tag{3.4}$$

Using the equilibrium condition for pure water,

$$\mu^{*}_{W,l}(T+\Delta T)=\mu^{*}_{W,g}(T+\Delta T,P+\Delta P) \tag{3.5}$$

and the Clausius–Clapeyron equation with constant heat of vaporization from the normal boiling point $T=T_{n.b.p.}$ as state 1 to a boiling point $T+\Delta T=T_{b.p.}$ as state 2,

$$\int_{1}^{2} d(\ln P)=-\frac{\Delta H}{R}\int_{1}^{2} d(1/T) \tag{3.6}$$

Then, Eq. (3.4) can be rearranged as

$$\Delta T_{b.p.}=\frac{-RT^{2}_{n.b.p.}/\Delta H\times\ln(1-x_U)}{1+RT_{n.b.p.}/\Delta H\times\ln(1-x_U)} \tag{3.7}$$

It can be clearly seen that Eq. (3.7) is reduced to Eq. (3.1) for $x_U<<1$. Equation (3.7) is exactly the same as the effective boiling point equation (Sirignano *et al.* (2008); Abu–Ramadan *et al.* (2011)) given by

$$\frac{1}{T_{b.p.}}-\frac{1}{T_{n.b.p.}}=\frac{R\ln x_W}{\Delta H} \tag{3.8}$$

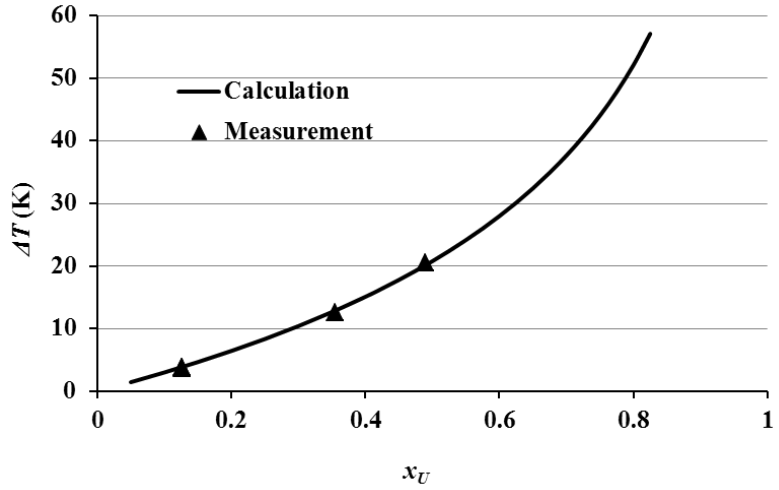

Figure 3.3 Prediction and measurement of boiling-point elevation of urea water mixture

To validate Eq. (3.7), samples with various urea molar fractions are prepared. To make samples, urea powders of 0 g, 50 g and 100 g are put into aqueous urea of 50 ml (37 g, 32.2 wt. %) which is equivalent to the molar fractions of urea, x_U of 0.126, 0.356, and 0.49. Figure 3.3 shows that Eq. (3.7) agrees well with our experimental data of the boiling-point elevation of the aqueous urea. The relative error is at most 3% which is estimated by:

$$\mathrm{err} = \frac{\left|\Delta T_{b.p.,cal} - \Delta T_{b.p.,exp}\right|}{\Delta T_{b.p.,cal}} \tag{3.9}$$

3.4 Heat transfer induced water vaporization

The heat required to vaporize water from the aqueous urea is transferred from the surroundings, and the convective heat transfer plays a major role in SCR applications. The incident heat is firstly used for phase change from the liquid water of the mixture to water vapor, and then for raising the water vapor temperature from the droplet surface temperature T_s to the surrounding gas temperature T_g as well as the mixture temperature. If the heat transfer rate is defined except the sensible heat for water vapor, it follows that

$$\dot{Q}_s = \dot{m}(-\Delta H') + mc\dot{T} \tag{3.10}$$

where m is the mass of the solution, c and T are its specific heat and temperature, respectively, and $\Delta H'$ is the corrected heat of vaporization considering the endothermic enthalpy of urea dissolution in water.

With an assumption that aqueous urea remains in the saturated solution during water evaporation, the temperature change rate $\dot{T}$ of the solution is the same as $\Delta\dot{T}_{b.p.}$. Since the amount of non-volatile urea in the solution remains the same, the current mass and its change rate are expressed as

$$m = \left(\frac{M_W}{M_U} \frac{1 - x_U}{x_U} + 1 \right) m_U \quad \text{and} \quad \dot{m} = -\frac{M_W}{M_U} \frac{\dot{x}_U}{x_U^2} m_U \tag{3.11}$$

respectively, with the current mole fraction of urea x_U, then Eq. (3.10) can be rewritten as

$$\frac{\dot{Q}_s dt}{m_U} = \left[\frac{M_W}{M_U} \frac{\Delta H'}{x_U^2} + \left(\frac{M_W}{M_U} \frac{1-x_U}{x_U} + 1 \right) c \frac{d\Delta T_{b.p.}}{dx} \right] dx \qquad (3.12)$$

where, M_W and M_U are molecular weights of water and urea. By integrating Eq. (3.12), the history of $x_U(t)$ can be obtained for a given heat supply $\dot{Q}_s$ with correctly modified $\Delta H'$.

The urea dissolution in water is known as an endothermic process, and the differential heat of solution of urea in infinite dilution of aqueous urea at 25℃ and 1 bar is 15.1 kJ/mol of urea. On the other hand, when water evaporates from the aqueous urea, the heat of water vaporization is reduced due to the dissolution heat of urea. The average decrease in the heat of water vaporization is 2.2 kJ/mol of water for the solution of the initial concentration 32.2 wt. % of urea. This is about 5% of the heat of water vaporization but cannot be ignored because of the accumulative effect.

Equation (3.12) is verified by comparing with experiments on water vaporization from the aqueous urea as shown in Fig. 3.4 where the variation of solution temperature is plotted according to the scale time. The scaled time is introduced to normalize time because the right hand side of Eq. (3.12) is independent of the amount of heat supply and initial sample mass. The scaled time t^* is defined for a constant heat supply as,

$$t^* = \int_0^t \frac{\dot{Q}_s}{m_U} dt = \frac{m\bar{c}(\Delta T/\Delta t)}{m_U} t = \frac{\bar{c}(\Delta T/\Delta t)}{Y_{U0}} t \qquad (3.13)$$

where, $\bar{c}$ is the average sensible specific heat of mixture and Y_{U0} is the initial urea mass fraction. $\Delta T/\Delta t$ is a slope from measurement for sensible heating. With Eq. (3.13), the actual heat supply from the gas burner can be implicitly obtained. Two samples of the aqueous

urea 150 ml, 32.5 wt. % of urea are heated at different rates of heat supply $\dot{Q}_s$. The supplied heat $\dot{Q}_s$ is calculated based on the average slope before boiling with the average specific heat of the aqueous of urea $\bar{c}$ =3.7 kJ/kg, $(\Delta T/\Delta t)_{\exp 1}$=0.172 K/s and $(\Delta T/\Delta t)_{\exp 2}$ =0.275 K/s. Since a small amount of water evaporates before boiling, the first boiling-points are different though their initial concentrations are the same. To correct the evaporation during the sensible heat supply, the reference time is shifted to match the boiling-point elevation of 10 K. The Watson relation (Polling *et al.* (2001)) is used to evaluate the heat of enthalpy of water, and the modified heat enthalpy is by adding ΔH_{DISS} =-2.2 kJ/mol as

$$\Delta H' = \Delta H_{n.b.p.}\left(\frac{T_c - T}{T_c - T_{n.b.p.}}\right)^{0.38} + \Delta H_{DISS} \tag{3.14}$$

where T_c =647 K, $T_{n.b.p.}$ =373 K, and $\Delta H_{n.b.p.}$ =40.7 kJ/mol.

Figure 3.4 shows that the calculation with the correction of enthalpy of urea dissolution agrees well with the experiments except at higher temperatures. This is because the urea decomposition begins when the temperature reaches at around 150℃.

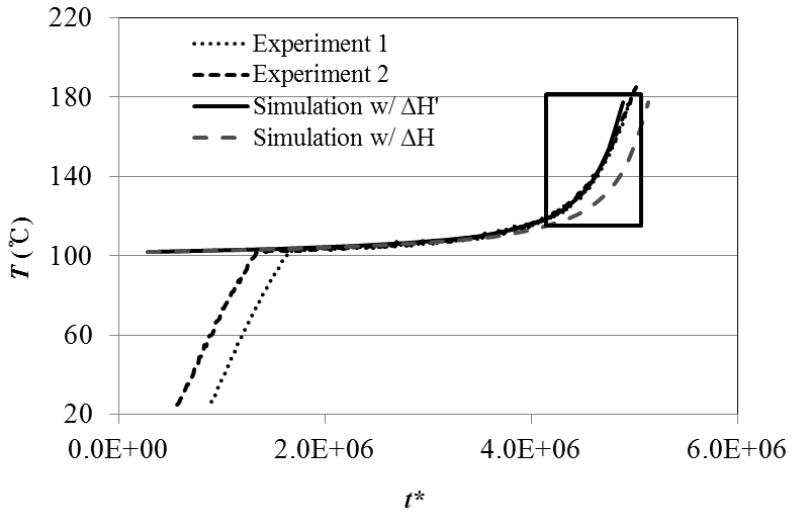

(a)

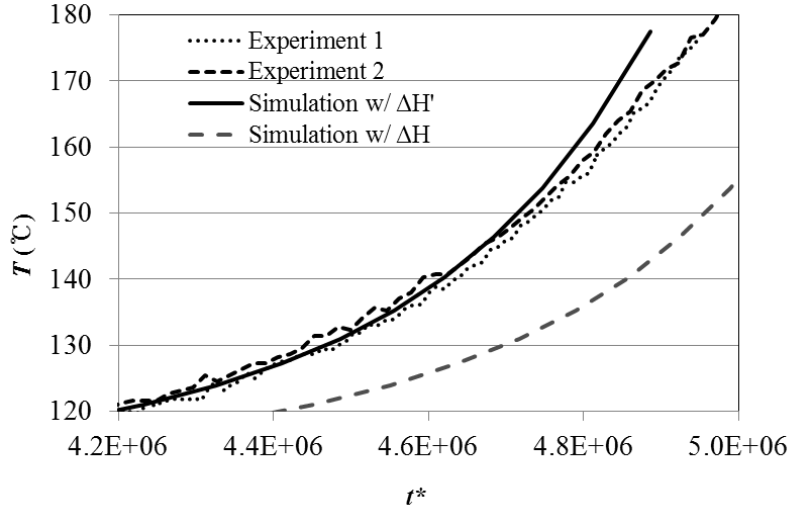

(b)

Figure 3.4 Temperature history of urea water solution with constant heat supply; Figure 3.4 (b) is the magnification of the data in the box in Fig. 3.4 (a).

3.5 Water vaporization from an aqueous urea droplet under free convection

On the condition of a stationary evaporation process, the vaporization relation of a droplet can be derived from energy balance. Since water has a high heat of vaporization so that the Spalding heat transfer number is small, the classical model for the droplet evaporation can be applied (Sazhin, S.S. (2006)). When the size and temperature of a droplet are assumed to vary slowly compared to the time scale required to reach a stationary condition, the rapid mixing model can be adopted for the internal mass diffusion and heat transfer of the droplet since the model gives the practically the same result with other complicated models such as the diffusion limit model (Birkhold et al. (2006)).

The heat and mass transfer analogy can exactly be satisfied when $\varphi = c_{pv} Sh_0 / c_{pg} Nu_0 Le_g = 1$ (Sazhin, S.S. (2006)), which is widely accepted in the analysis of droplet evaporation in the dry surrounding gas. Detailed derivation for φ is discussed in Appendix A.4. In this study, $\varphi = 1.26$ at 373 K for a dry condition. Despite the discrepancy, the heat and mass transfer analogy is used for practical reasons such as simplicity in measuring temperature and heat transfer rate and lack of the diffusivity data of some molecules in various temperature ranges if chemical reactions take place during the urea−SCR process. It is ignored that the sensible heat in the initial transient period associated with the droplet heating to the boiling point because Wang *et al.*'s experiment (2009) showed that the transient period is so short for about $t/D_0^2 < 2$ that a noticeable decrease in the droplet diameter can hardly be observed. The effect of initial sensible heating process on evaporation will be discussed later in this section.

With those assumptions, water vaporization from an aqueous urea droplet can be described as follows. The Spalding heat transfer

number is the ratio of the heat required to move vapor from the droplet surface to the surroundings to the heat that reaches the surface, which is defined as

$$B_T = \frac{(-\dot{m}_d)c_{pv}(T_g - T_d)}{\dot{Q}_s} \tag{3.15}$$

where the subscript *d* stands for the droplet, and c_{pv} is the specific heat of water vapor at constant pressure. Using Eqs. (3.7), (3.10) and (3.11) $\dot{Q}_s/(-\dot{m}_d)$ can be expressed as follows,

$$\frac{\dot{Q}_s}{-\dot{m}_d} = \Delta H' - m_d c_d \frac{dT}{dx}\dot{x}_U = \Delta H' + m_d c_d \frac{dT}{dx}\frac{M_U}{M_W}\frac{x_U^2}{m_U} \tag{3.16}$$

where dT/dx is the derivative of Eq. (3.7). Since the mole fraction of urea is a function of the drop mass $x_U = x_U(m_d)$ in Eq. (3.11), the transfer number can be written as a function of the droplet mass and the surrounding temperature, $B_T(m_d, T_g)$. The specific heat of water and the properties of air are evaluated at the mean temperature $(T_d + T_g)/2$. The density and specific heat of the droplet are assumed to be composition dependent as,

$$\rho_d = 950(1 - Y_U) + 1300Y_U \tag{3.17}$$

$$c_d = 4200(1 - Y_U) + 3000Y_U \tag{3.18}$$

The classical model based on the film theory anticipates the rate of mass change of a droplet as,

$$\dot{m}_d = -\pi D_d \frac{k_g}{c_{pv}} \overline{Nu}_0 \ln(1+B_T) \tag{3.19}$$

where $\overline{Nu}_0$ is the Nusselt number for a non-evaporating droplet. Since the drop diameter $D_d = \sqrt[3]{6m_d/\pi\rho_d}$ is also a function of m_d like the transfer number $B_T(m_d, T_g)$, Eq. (3.19) can easily be integrated with an ordinary differential equation solver. Note that Eq. (3.19) can be expressed in terms of D_d^2 when dividing Eq. (3.19) by D_d as follows;

$$\frac{dD_d^2}{dt} + \frac{2}{3}\frac{d\ln\rho_d}{dt} D_d^2 = -\frac{4k_g}{\rho_d c_{pv}} \overline{Nu}_0 \ln(1+B_T) \tag{3.20}$$

The second term on the left hand side of Eq. (3.20) accounts for the mixture density variation, but its influence is becoming weaker as the diameter D_d decreases. However, as the magnitude of the drop density on the right hand side increases by about 30% compared to the initial density, the time-derivative of D_d^2 is not steep at the final stage. In the present calculation, Eq. (3.19) is used because of simplicity, but the data are plotted in terms of D_d^2 by converting m_d data to compare with literature data.

In the case of natural convection, the Churchill's correlation for spheres in fluid for $Pr \geq 0.7$ and $Ra_{D_d} \leq 10^{11}$ is given by (Incropera *et al.* (2007))

$$\overline{Nu}_0 = 2 + \frac{0.589 Ra_{D_d}^{1/4}}{\left[1+(0.469/Pr)^{9/16}\right]^{4/9}} \tag{3.21}$$

where Ra_{D_d} is the Rayleigh number defined as $Ra_{D_d} = \frac{g\beta_g |T_d - T_g| D_d^3}{\nu_g \alpha_g}$ and Pr is the Prandtl number. The Nusselt number is also a function of drop mass and surrounding temperature, $\overline{Nu}_0(m_d, T_g)$.

Equations (3.15), (3.16) and (3.21) are plugged in Eq. (3.19) and it is integrated with an ordinary differential equation solver called the lsode routine in GNU Octave (Eaton *et al.* (2011)). The lsode routine is based on a multi-step method and internal time step is controlled to guarantee to deal with stiff problems. Figures 3.5 and 3.6 show the droplet evolutions at the surrounding temperatures of 200℃ and 300℃ respectively. Wang *et al.* (2009) conducted experiments with aqueous urea droplets whose diameter were less than 1 mm with 32.5 wt.% of urea, and Musa *et al.* (2006) considered drops of larger than 2 mm with 30 wt.%. Both groups performed vaporization experiments of droplets suspended from a quartz fiber in an electrical furnace. In Figs. 3.5 and 3.6, the trend of droplet size variation is only depicted not all the scattered data from those measurements. The wide discrepancies between the two measurements have not been clearly explained so far.

The water evaporation is confirmed to follow the D^2-law for the measurements and calculations since the transfer number is small due to large latent heat of water, and the temperature change is not high during most evaporation process. As previously discussed with Eq. (3.20), Figs. 3.5 and 3.6 show that the final slope of D^2 curve is not so steep as the initial slope. The temperature of droplets of 0.87 mm at 200℃ and 0.923 mm at 300℃ is marked on the diameter evolution line. It is noted that the temperature rise of a droplet is accelerated at the final stage of evaporation, since the drop mass is so small that its temperature easily increases due to smaller heat capacity of the droplet after water evaporation.

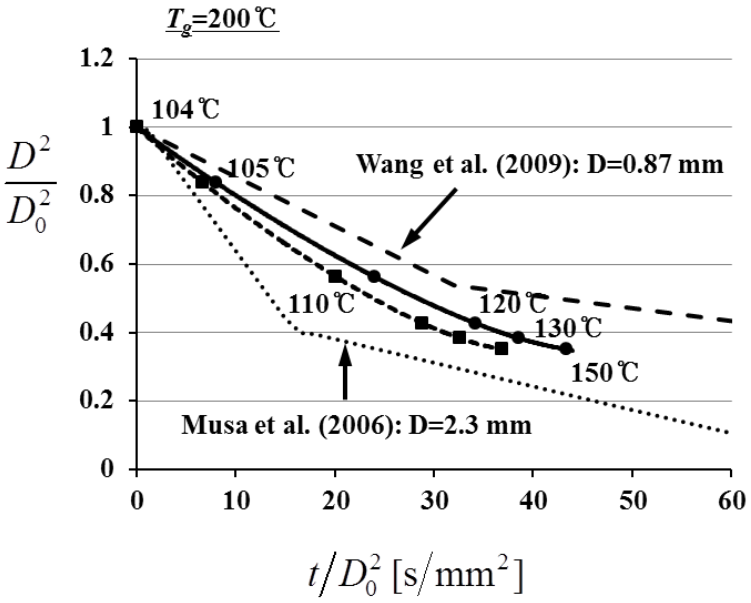

Figure 3.5 Evolution comparison of aqueous urea drop for the environment temperature 200℃ with the experiments of Wang et al. (2009) and Musa et al. (2006)

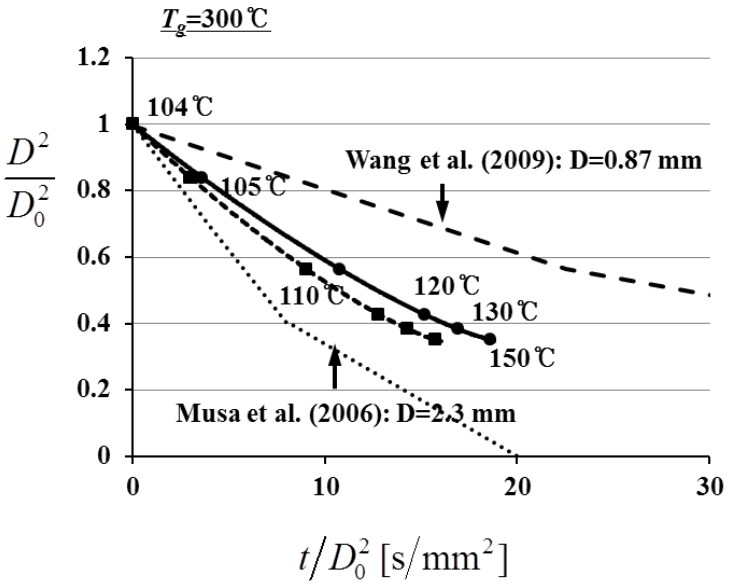

Figure 3.6 Evolution comparison of aqueous urea drop for the environment temperature 300℃ with the experiments of Wang et al. (2009) and Musa et al. (2006)

The initial sensible heating process has been ignored by assuming that the time duration is short and the amount of evaporated water is small. Without evaporating water, droplet temperature is calculated as:

$$c_{pd} m_d \frac{d\left(T_g - T_d\right)}{dt} = \pi D_d k_g \overline{Nu}_0 \left(T_g - T_d\right) \tag{3.22}$$

On the other hand, Birkhold *et al.* (2007) and Strom *et al.* (2009) adopted models that water evaporates during sensible heating process. The model of Birkhold *et al.* (2007) is discussed in Appendix A.4. They used heat transfer number as a governing equation.

Figure 3.7 shows that mass trends of Birkhold *et al.* (2007) and the current study are similar to each other. However, the temperature histories are quite different in Fig. 3.8. It is worth noting that the temperature of a pure water droplet is constant that is not physical though the Kelvin effect on evaporation is taken into account. Birkhold *et al.* (2007) model is not valid near the boiling point as well as shown in the definition of mass transfer number. It is also worth noting that the initial slopes of the models are the same. Birkhold et al. (2007) model is recalculated; any singularity around the temperature 340 K is not detected.

Based on the temperature given by Eq. (3.22), water evaporation is calculated and shown in Fig. 3.9. 12% of water evaporation is found to be ignored and the result agrees well with recalculated Birkhold model in Fig. 3.8. Water evaporation during sensible heating process is ignored in CFD implementation described in the next section since the effect is small.

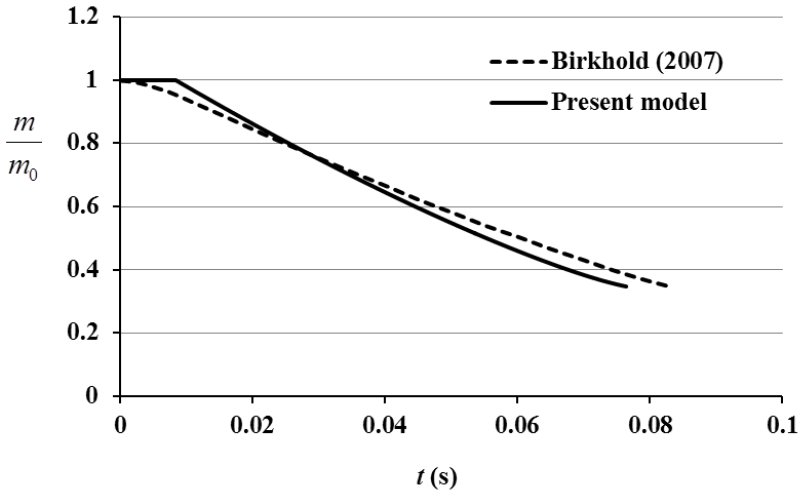

Figure 3.7 Mass history for a droplet under free convection: T_{d0}=300 K, T_g=673 K, p_g=0.11 MPa, D_{d0}=70 μm

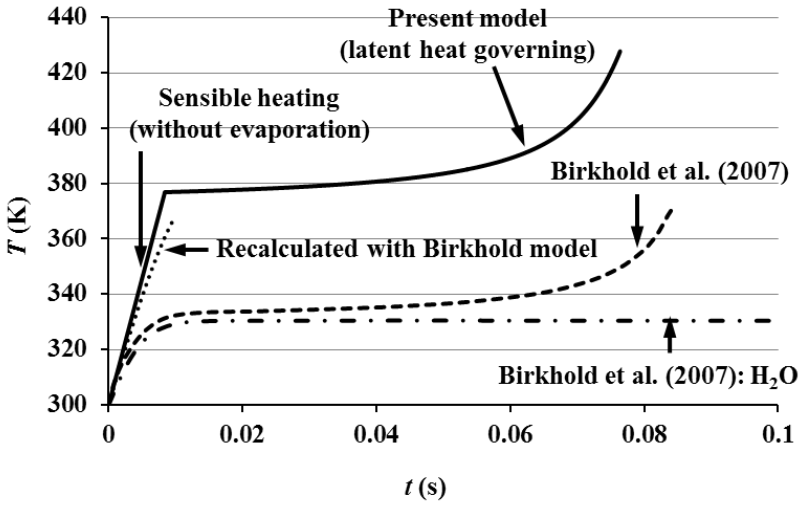

Figure 3.8 Temperature history for a droplet under free convection: T_{d0}=300 K, T_g=673 K, p_g=0.11 MPa, D_{d0}=70 μm

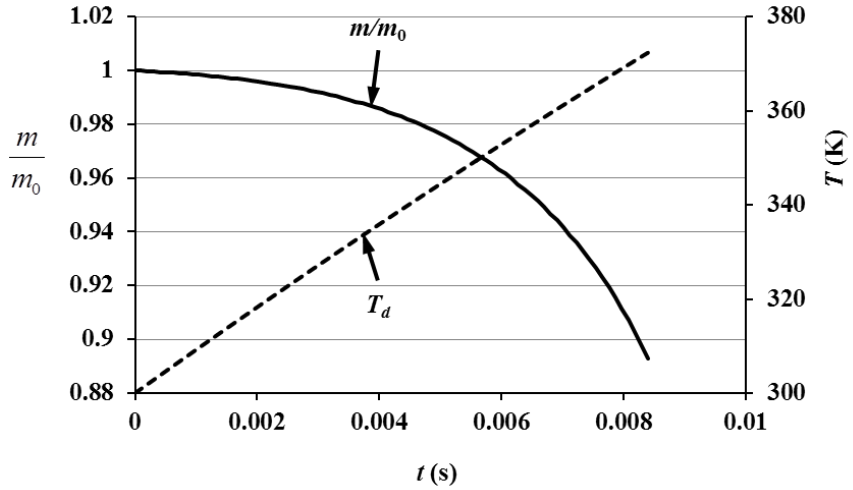

Figure 3.9 Droplet mass change based on the temperature with an assumption of no water evaporation

3.6 Water vaporization from an aqueous droplet under forced convection

When an aqueous urea droplet is injected in the exhaust gas stream, it interacts with the carrier flow. As discussed in the previous section for heat and mass transfer, it takes energy from the surrounding gas and gives water vapor back. Momentum transfer is also involved for forced convection analysis. One of numerical methods to deal with discrete particles in continuous medium is Euler–Lagrange approach.

The Euler–Lagrange approach is a simulation method where the equations of motion, energy and species for the continuous phase are solved on an Eulerian frame of reference and the governing equations for the disperse phase are dealt in a Lagrangian frame of reference. The OpenFOAM(Open Field Operation and Manipulation) CFD code is selected to analyze a two–phase problem for the dynamics of aqueous urea droplets in the exhaust channel. The OpenFOAM CFD toolbox is a free, open source CFD software package and it has extensive features to solve problems of complex fluid flows involving chemical reactions, turbulence and heat transfer. It provides template code to deal with droplets in a flow. Since temperature range from the surrounding gas to droplets or walls is broad, compressible flow solver is adopted. The energy equation used in the analysis is summarized in Appendix A.5.

For Eulerian description for particles heat and mass transfer relations are implemented as described in the previous section for natural convection environment. Equation (3.22) describes droplet heat transfer during sensible heating process and Eq. (3.19) describes heat and mass transfer during weakly sensible and latent heat process. Core source code for heat and transfer is listed in Appendix B.4. Droplet kinematics is summarized in Appendix A.3.

$$m_P \frac{d\vec{U}_P}{dt} = \vec{F}_D + m_P \vec{g} = -C_D \frac{1}{2} \left| \vec{U}_P - \vec{U}_c \right| \left(\vec{U}_P - \vec{U}_c \right) + m_p \vec{g} \qquad (3.23)$$

Forces due to shear and gravity are assumed to be exerted on a particle as in Eq. (3.23). Drag coefficient is consulted in Appendix A.3.

A source code is developed and plugged in OpenFOAM based on the present study. The behavior of aqueous urea droplets is investigated with the code. The droplets are radially injected 50 mm off the center of the channel of 300 mm diameter in Fig. 3.10. The channel geometry is adopted from Kim *et al.* (2004) but the injector properties such as radial mass distribution follow the work of Birkhold *et al.* (2006). One-way interaction from the carrier flow to droplets is considered since the ratio of injection mass of aqueous urea to carrier flow is small. The number of particles is injected about 80,000 for 0.03 s.

Figure 3.11 shows that time taken to reach at the boiling point and water depletion with respect to initial droplet diameter. Depletion data are scattered since the injection angle for each droplet is randomized and the travel and interaction in the carrier flow are different from each other. Droplet temperature at the injector is T_d=300 K and the carrier flow temperature is T_d=473 K. The carrier flow speed along the axial axis is 30 m/s. It is shown in Fig. 3.11 the duration for reaching at the boiling point is about one-tenth of the total duration for water depletion. It is also guessed form Fig. 3.11 that a droplet of initial diameter 100 μm can travel long distance and it may come to hit the internal surface of the channel in a compact SCR system.

Parameter studies for the temperature and velocity of the carrier flow is performed to analyze their influence on water depletion. By extracting average time from CFD simulation temperature and velocity influences are clearly depicted. The temperature effect of the carrier flow range from 473 K to 613 K in Fig. 3.12 shows that the depletion

time is inversely proportional to the difference between temperatures of droplet and the carrier flow. It is the same relation to the parameter study on velocity difference between droplet and the carrier flow. It is because the driving force for energy transfer is proportional to temperature difference and the square root of velocity difference.

In this section the proposed model for water depletion from an aqueous droplet is shown to work well with OpenFOAM code and it can be concluded that the model works with current CFD practices as well.

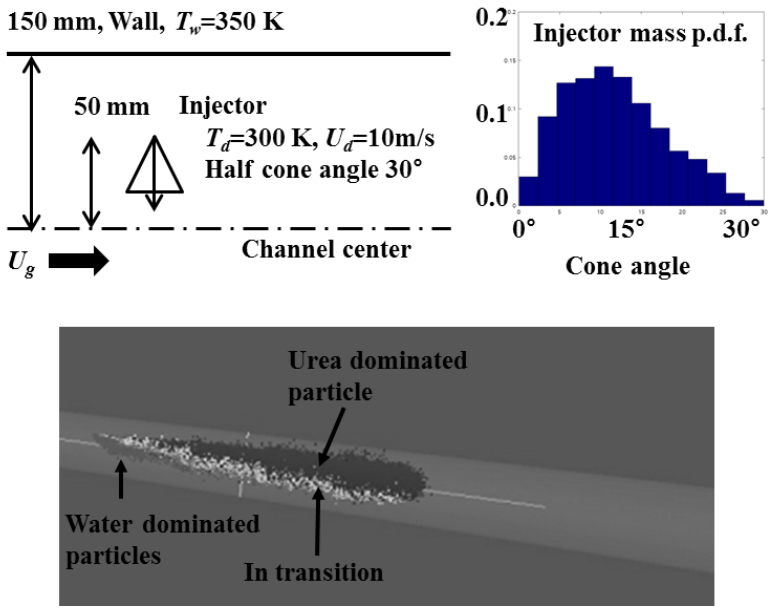

Figure 3.10 CFD simulation of aqueous urea injection

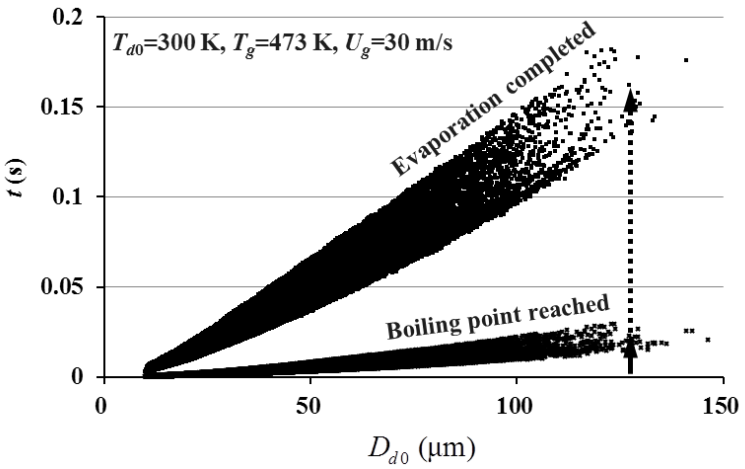

Figure 3.11 Time scattering to boil and deplete water with respect to initial droplet diameter

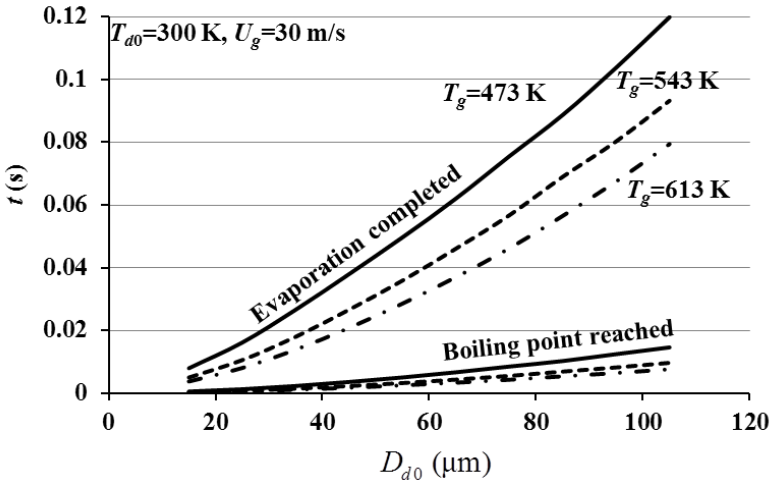

Figure 3.12 Parameter study for surrounding gas temperature: average time to boil and deplete water from a droplet

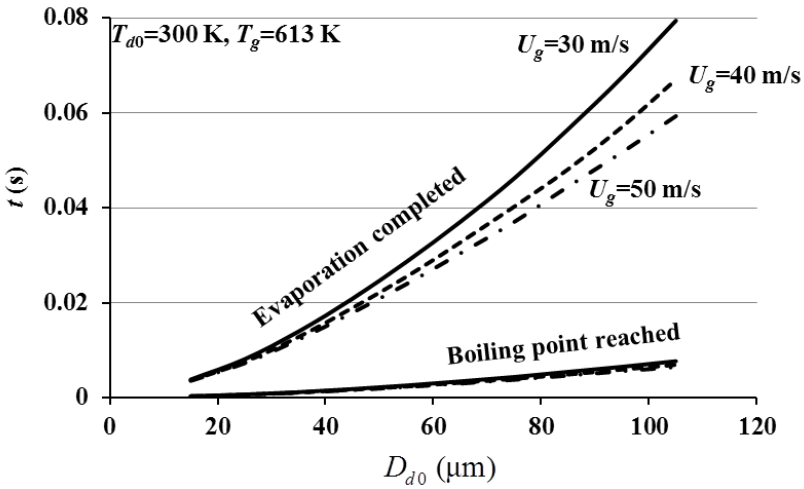

Figure 3.13 Parameter study for surrounding gas velocity: average time to boil and deplete water from a droplet

3.7 Summary

A model is proposed for water vaporization from aqueous urea, which takes into account of boiling-point elevation, and applied this model to water evaporation from an aqueous urea droplet. The results are summarized as follows;

1) The boiling-point elevation is expressed as a function of the mole fraction of urea, which turns out to be equivalent to the effective boiling point proposed by Sirignano and Wu (2008). The model is validated by experiments. The temperature change of the urea mixture should not be ignored for appropriate description of the aqueous urea behavior since the boiling-point increases significantly as water evaporates.

2) A model for water vaporization from aqueous urea is proposed, which agrees well with experiments. The correction regarding the enthalpy of urea dissolution in water is crucial to describe the water vaporization since its effect is accumulated.

3) The proposed model for water depletion is shown to work well with conventional CFD practices by implementation in OpenFOAM code. Water depletion time is inversely proportional to the temperature and velocity difference between a droplet and the carrier flow.

4) Finally, the water vaporization model with the boiling-point elevation relation is applied to the vaporization of aqueous urea droplets. As a result, it is found that urea decomposition begins before water evaporation finishes due to boiling-point elevation.

Chapter 4
Summary and Conclusion

Air pollution from internal engines has serious impacts on the environment and health around the world, especially in urban are. Many countries around the world set up emission standards to cope with the situation and engine manufacturers are trying to cope with the emission regulations. Nitrogen oxides are subject under control by the regulations, one of practically available ways to reduce NOx emission is selective catalytic reduction using aqueous urea.

Urea-SCR technology uses aqueous urea that should be converted into ammonia in the exhaust stream. Converting processes begin with the sprayed injection of urea in the stream. Some of injected droplets reach the surface of the channel and form deposits. This study is a fundamental research on chemical reactions and thermos-physical properties of urea and its role in the water solvent to understand the deposit formation.

A urea pyrolysis model for the temperature around 200℃ is developed to describe deposition on the surface of the SCR system. With the model and its kinetic parameters set from experiments, the model gives the following observations:

1) The temperature and specific surface area are main factors to determine the amount of deposits. The competition depending on those factors between the formation of cyauric acid and evaporation of isocyanic acid determines the amount of deposits.
2) The terminal quantity of deposits, mainly cyanuric acid, increases at higher reaction temperature and deeper depth of the film.

Water vaporization from aqueous urea is a first process during the conversion of urea into ammonia. Two colligative properties for

describe water evaporation are examined: boiling-point elevation and change in heat of vaporization of water from aqueous urea. The heat and mass transfer model for a droplet in the surrounding gas is proposed. The model for droplet evaporation analysis reveals the following observations:

1) The relation of boiling-point elevation indicates that the temperature change of the urea mixture should be included for describing aqueous urea behavior.
2) The correction of heat of vaporization of water in aqueous urea due to the enthalpy of urea dissolution in water is needed to describe the water vaporization.
3) Urea decomposition can begin before water evaporation finishes due to boiling-point elevation rise as the urea fraction increases.

Reference

Abramzon, B. and Sirignano, W.A., Droplet vaporization model for spray combustion calculations, Int. J. Heat Mass Transfer, 32 (9) (1989) 1605-1618

Aggarwal, S.K. and Peng, F., A review of droplet dynamics and vaporization modeling for engineering calculations, Journal of Engineering for Gas Turbines and Power, 117, (1995) 453-461

Aoki, H., Fujiwara, T., Morozumi, Y., Miura, T., Measurement of urea thermal decomposition reaction rate for NO selective non-catalytic reduction, Proceedings of 5th International Conference on Technologies and Combustion for a Clean Environment. Lisbon, Portugal, 1 (1999) 115-118

Abu-Ramadan, E., Saha, K. and Li, X., Modeling the depleting mechanism of urea-water-solution droplet for automotive selective catalytic reduction systems, AIChE j. 57 (2011) 3210-3225

Bernhard, A.M., Peitz, D., Elsener, M., Wokaun, A. and Krocher, O., Hydrolysis and thermolysis of urea and its decomposition byproducts biuret, cyauric acid and melamine over anatase TiO2, Appl. Catal., B Environ. 115-116 (2012) 129-137

Birkhold, F., Meingast, U. and Wassermann, P. Analysis of the injection of urea-water-solution for automotive SCR DeNOx-systems: modeling of two-phase flow and spray/wall interaction, SAE paper, (2006) No. 2006-01-0643

Birkhold, F., Meingast, U., Wassermann, P. and Deutschmann, O., Modeling and simulation of the injection of urea-water-solution for automotive SCR DeNOx-systems, Appl. Catal., B Environ. 70 (2007) 119-127

Brack, W., Heine, B., Birkhold, F., Kruse, M., Schoch, G., Tischer, S. and Deutschmann, O., Kinetic modeling of urea decomposition based on systematic thermogravimetric analysis of urea and its most important byproducts, Chemical Engineering Science, 106 (2014), 1-8

Eaton, J.W., Bateman, D., Hauberg, S. and Wehbring, R., GNU Octave version 3.8.0 manual, from http://www.gnu.org/software/octave/octave.pdf (2011)

Eichelbaum, M., Farrauto, R.J. and Castaldi, M.J. The impact of urea on the performance of metal exchanged zeolites for the selective catalytic reduction of NOx, Part I. Pyrolysis and hydrolysis of urea over zeolite catalysts, Appl. Catal., B Environ. 97 (2010) 90-97

Fang, H.L. and DaCosta, H.F.M., Urea thermloysis and NOx reduction with and without SCR catalysts, Appl. Catal., B Environ. 46 (2003) 17-34

Feng. Z-G., and Michaelides, E.E., Drag coefficients of viscous spheres at intermediate and high Reynolds numbers, J. Fluids Eng., 123 (2001) 841-849

Grout, S., Blaisot, J.-B., Pajot, K. and Osbat, G. Experimental investigation on the injection of a urea-water solution in hot air stream for the SCR application: Evaporation and spray/wall interaction,

Fuel, 106 (2013) 166-177

Incropera, F.P., DeWitt, D.P., Bergman, T.L. and Lavine, A.S., Fundamentals of Heat and Mass Transfer, 6th Ed. John Wiley & Sons. NY, USA (2007)

Kim, J.Y., Ryu, S.H. and Ha, J.S., Numerical prediction on the characteristics of spray-induced mixing and thermal decomposition of urea solution in SCR system, fall conference ASME Internal Combustion Engine Division, ICEF2004-889 (2004)

Koebel, M. and Strutz, E.O., Thermal and hydrolytic decomposition of urea for automotive selective reduction systems: thermochemical and practical aspects, Ind. Eng. Chem. Res. 42 (2003), 2093-2100

Levine, I.N, Physical chemistry, 5th ed., McGraw-Hill (2002)

Lundstrom, A., Andersson, B. and Olsson, L., Urea thermolysis studied under flow reactor conditions using DSC and FT-IR, Chemical Engineering Journal 150 (2009) 544-550

Musa, S., Saito, M., Furuhata, T. and Arai, M., Evaporation characteristics of a single aqueous urea solution droplet, ICLASS, Paper ID ICLASS06-195 (2006)

Poling, B.E., Prausnitz, J.M. and O' Connell, J.P., The properties of gases and liquids, 5th Ed. McGraw-Hill, NY, USA (2001)

Ryddner, D.T. and Trujillo, M.F., Modeling urea-water solu-tion droplet evaporation, Emiss. Control Sci. Technol, 1 (2015) 80-97

Sazhin, S.S., Advanced models of fuel droplet heating and evaporation, *Progress in Energy and Combustion Science*, 32, (2006) 162-214

Schaber, P.M., Colson, J., Thielen, D., Anspach, B. and Brauer, J., Thermal decomposition (pyrolysis) of urea in an open reaction vessel, Thermochimica Acta 424 (2004) 131-142

Sirignano, W.A. and Wu, G., Multicomponent-liquid-fuel vaporization with complex configuration, Int. J. Heat Mass Transfer, 51 (2008) 4759-4774

Strom, H., Lundstrom, A., and Andersson, B., Choice of urea-spray models in CFD simulations of urea-SCR systems, Chemical Engineering Journal, 150 (2009) 69-82

Strots, V.O., Santhanam, S., Adelman, B.J., Griffin, G.A. and Derybowski, E.M., Deposit formation in urea-SCR systems, SAE Int. J. Fuels Lubr. SAE 2009-01-2780

Wang, T.J., Baek, S.W., Lee, S.Y., Kang, D.H. and Yeo, G.K., Experimental investigation on evaporation of urea-water-solution droplet for SCR applications, AIChE J. 55 (2009) 3267-3276

White, F.M., Viscous fluid flow, 3rd ed., McGraw-Hill (2006)

Yim, S.D., et al, Decomposition of Urea into NH3 for the SCR process, Ind. Eng. Chem. Res. 43 (2004), 4856-4863

Zanoelo, E.F., A lumped model for thermal decomposition of urea. uncertainties analysis and selective non-catalytic reduction of NO, Chemical Engineering Science 64 (2009) 1075-1084

Appendix A

A.1 Effusion equation for isocyanic acid

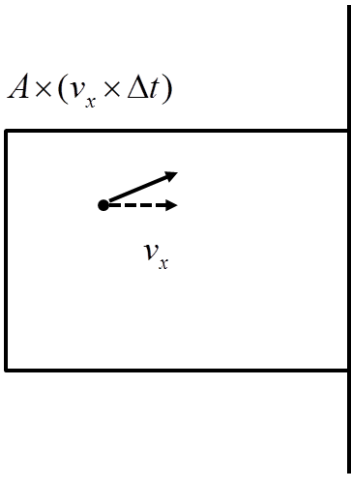

Figure A.1 A box containing molecules that strike the right wall

For a liquid in equilibrium with its vapor, the rate of evaporation of liquid molecules equals the rate of condensation of gas molecules. Based on an assumption that every vapor molecule strikes the surface of the liquid condenses to liquid and the same amount of molecules in liquid phase leave the liquid, effusion equation is induced from the collision flux. The collision flux Z_w can be interpreted as the rate of leaving molecules and it can be derived from the theory of gas kinetics.

Consider a molecule with the velocity $v_x > 0$ in a box as shown in Fig. A.1. The molecule travels $v_x \times \Delta t$ and strikes the wall in Δt and the number of molecules that hit the wall $N_w(v_x)$ within the volume

$A\times(v_x\times\Delta t)$ is as follows:

$$dN_w(v_x)=(Av_x\Delta t)\frac{N}{V}f(v_x)dv_x \tag{A.1}$$

where the number of molecules in the system volume V is N, and N/V is the density of molecules. The Maxwell distribution function for v_x is as:

$$f(v_x)dv_x=\left(\frac{m}{2\pi kT}\right)^{1/2}\exp\left[-\frac{mv_x^2}{2kT}\right] \tag{A.2}$$

Then the collision flux Z_w is obtained by integrating Eq. (A.1) for $v_x>0$ as follows:

$$Z_w=\lim_{\Delta t\to 0}\frac{1}{A\Delta t}\int_{v_x>0}dN_w=\frac{N}{V}\int_0^\infty v_x f(v_x)dv_x=\frac{1}{4}\frac{N}{V}\langle v\rangle \tag{A.3}$$

or, it can be explicitly expressed as:

$$Z_w=\frac{1}{4}\frac{PN_A}{RT}\left(\frac{8RT}{\pi M}\right)^{1/2} \tag{A.4}$$

where, N_A is the Avogardo number and M is molecular mass. Equation (A.4) gives the temperature dependency and shows that the collision flux is proportional to $T^{-1/2}$.

The collision flux equation is used to describe the escape of gas through a tiny hole in the wall, which is called effusion. The flux

equation can be also applied to describe the kinetics of evaporation. In the case of absence of the escaping molecule in the surrounding gas, the rate of evaporation per unit area is exactly the same as the collision flux equation. Using the Clausius–Clapeyron equation with constant ΔH assumption, the pressure for liquid–gas equilibrium is as follows:

$$\ln \frac{P}{P_1} = -\frac{\Delta H}{R}\left(\frac{1}{T} - \frac{1}{T_1}\right) \tag{A.5}$$

On the other hand, for dilute solution ideal vapor pressure is proportional to mole fraction of the escaping molecules, or Henry law says:

$$P_i = K_i x_i^l \tag{A.6}$$

where, K_i is a proportional constant and x_i^l is the mole fraction of species i in the liquid solution.

Equations (A.4), (A.5) and (A.6) lead the equation of evaporation of isocyanic acid in the mixture by putting all constants into a constant B except heat of vaporization ΔH and the gas constant, and the variable temperature T. The evaporation of isocyanic acid is restated here:

HNCO (l) → HNCO (g) (2.7)

$$\frac{dn_{I,e}}{dt} = -A\beta \frac{n_I}{n_T} \tag{2.8}$$

where n_I is a molar quantity of isocyanic acid and the subscript e represents evaporation, and the kinetic constant β is defined as:

$$\beta = \frac{B}{\sqrt{T}} \exp\left[-\frac{\Delta_{lg} H_{HNCO}}{RT} \right] \tag{2.9}$$

The enthalpy of vaporization is put for calculation of this thesis $\Delta_{lg} H_{HNCO} = 20.6$ kJ/mol and B is obtained from fitting by experiments. In Table 2.1 the model and required parameters are summarized.

A.2 Bird correction for droplet evaporation from energy balance

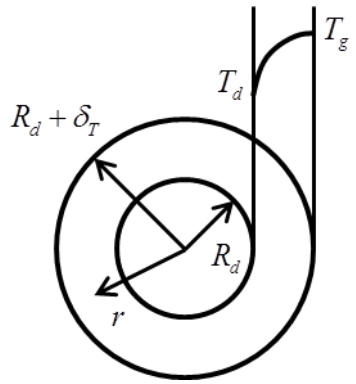

Figure A.2 Thermal film δ_T and the temperature around the droplet of a radius r

Let us assume that the thickness of thermal film is greater than that of diffusion film $\delta_T > \delta_D$ and it governs the diffusion. The inflow heat into the shell r in Fig. A.2 can be expressed as:

$$4\pi r^2 k_g \frac{dT}{dr} = -\dot{m}_d c_{pv}(T - T_s) - \dot{m}_d L(T_s) + \dot{q}_d \tag{A.7}$$

where L is the heat of vaporization and $\dot{q}_d$ is an internal heat source or enthalpy change of droplet. With an assumption of constant or average properties, Eq. (A.7) can be integrated from R_d to $R_d + \delta_T$ with the transfer number B_T:

$$-\frac{\dot{m}_d}{r}\Bigg|_{R_d}^{R_d+\delta_T} = -\frac{4\pi k_g}{c_{pv}}\ln(1+B_T) \tag{A.8}$$

$$B_T = \frac{c_{pv}(T_g - T_s)}{L(T_s) - \dot{q}_d/\dot{m}_d} \tag{A.9}$$

On the other hand, for non-evaporation, steady-state drops, constant heat transfer condition is written as follows:

$$-4\pi r^2 k_g \frac{dT}{dr} = 4\pi R_d^2 h_0 (T_s - T_g) \tag{A.10}$$

Equation (A.10) is integrated from R_d to $R_d + \delta_T$ and the result is put in Eq. (A.8). The final droplet evaporation equation from energy balance is obtained as:

$$\dot{m}_d = -\pi D_d \frac{k_g}{c_{pv}} Nu_0 \ln(1+B_T) \tag{A.11}$$

where D_d is the diameter of the drop. It is assumed that the evaporation process is quasi-steady in Eq. (A.11). Note that the rate of drop mass is negative. Let us define z as the ratio of the energy consumed to heat evaporated vapor from the surface temperature to the surrounding temperature to the incident energy from the surrounding gas:

$$z = \frac{-\dot{m}_d c_{pv} \Delta T}{\underbrace{4\pi R_d^2 h_0 \Delta T}_{\dot{q}_0}} = \frac{\dot{m}_d'' c_{pv}}{h_0} \tag{A.12}$$

and the transfer number is

$$B_T = \frac{c_{pv}\left(T_g - T_s\right)}{\underbrace{L(T_s) - \dot{q}_d / \dot{m}_d}_{\dot{q}_s}} = \frac{z\dot{q}_0}{\dot{q}_s} \tag{A.13}$$

then Eq. (A.11) turns $z = \ln\left(1 + z\dot{q}_0 / \dot{q}_s\right)$, or the well-known Bird correction equation:

$$\dot{q}_s = \dot{q}_0 \frac{z}{e^z - 1} \tag{A.14}$$

This correction is useful when dealing with an evaporating droplet as if non-evaporating droplet is handled.

A.3 Momentum equations for a particle in OpenFOAM code

The motion of particles is governed by the Newton equation. When the radio of carrier flow density to particle density is small $\rho_c/\rho_P << 1$, drag and gravity forces are dominating.

$$m_P \frac{d\vec{U}_P}{dt} = \sum \vec{F} = \vec{F}_D + m_P \vec{g} = -C_D \frac{1}{2} \left| \vec{U}_P - \vec{U}_c \right| \left(\vec{U}_P - \vec{U}_c \right) + m_p \vec{g} \tag{A.15}$$

The drag coefficient is in terms of the particle Reynolds number $Re_P = \left| \vec{U}_P - \vec{U}_c \right| D_P / \nu_c$ in the code:

$$C_D = \begin{cases} 0.424 & \text{for } Re_P > 1000 \\ \dfrac{24}{Re_P} \left(1 + \dfrac{1}{6} Re_P^{2/3} \right) & \text{for } Re_P \le 1000 \end{cases} \tag{A.16}$$

which is recommended for solid spheres in $Re_P \le 1000$ (Feng and Michaelides (2001); White, F.M. (2006)). During the simulation for small droplets $D_P \le 200\,\mu\text{m}$, the particle Reynolds number satisfies $Re_P \le 1000$.

On the other hand implicit Euler method is used for the ordinary differential equation of the form:

$$\frac{d(x-\alpha)}{dt} + \beta(x-\alpha) = 0 \tag{A.17}$$

Equation (A.17) is solved in the form of difference equation:

$$(x-\alpha)^{(n+1)} = \frac{(x-\alpha)^{(n)}}{1+\Delta t\beta^{(n+1)}} \tag{A.18}$$

Since the large number of particles takes part in the simulation, full implicit method is very expensive. If part of Eq. (A.15) is evaluated in the step (n), Eq. (A.18) can be used to gain extra stability compared to explicit Euler method.

$$\beta^{(n)} = \left(\frac{C_D}{m_P} \frac{1}{2} \left| \vec{U}_P - \vec{U}_c \right| \right)^{(n)} \tag{A.19}$$

$$\alpha^{(n)}\beta^{(n)} = \beta^{(n)}\vec{U}_c^{(n)} - \vec{g} \tag{A.20}$$

Then Eq. (A.18) is written as:

$$\left(x^{(n+1)} - \alpha^{(n)}\right) = \frac{\left(x^{(n)} - \alpha^{(n)}\right)}{1+\Delta t\beta^{(n)}} \tag{A.21}$$

Equation (A.15) is implemented in the code listed in Codes A.1 and A.2. Detailed implantation should be consulted in the full code list. Momentum transfer from the particle to the carrier phase is calculated by the variable dUTrans in the last line of Code A.1.

In a Lagrangian frame, each particle position vector $\vec{x}_P$ is obtained by integrating the equation:

$$\frac{d\vec{x}_P}{dt} = \vec{U}_P \tag{A.22}$$

The particle position is updated by the explicit Euler scheme.

$$\vec{x}_P^{(n+1)} = \vec{x}_P^{(n)} + \vec{U}_P^{(n)}\Delta t$$

(A.22)

The velocity at (n) step is used in Eq. (A.22) to keep the particle within its current cell. Cross-border movement is done in a separate iteration. Since the incremental time step Δt is calculated considering current cell condition prior to update velocity, the particle velocity at (n+1) cannot be used for calculating Eq. (A.22). One needs to consult **trackToFace()** routine to understand the mechanism in detail.

Code A.1 Foam::KinematicParcel<ParcelType>::calcVelocity

```
    // New particle velocity
    //~~~~~~~~~~~~~~~~~~~~~~

    // Update velocity - treat as 3-D
    const vector abp = (Feff.Sp()*Uc_ + (Feff.Su() +
Su))/massEff;
    const scalar bp = Feff.Sp()/massEff;

    Spu = dt*Feff.Sp();

    IntegrationScheme<vector>::integrationResult Ures =
        td.cloud().UIntegrator().integrate(U_, dt, abp, bp);

    vector Unew = Ures.value();

    // note: Feff.Sp() and Fc.Sp() must be the same
    dUTrans += dt*(Feff.Sp()*(Ures.average() - Uc_) - Fcp.Su());
```

Code A.2 Foam::Euler<Type>::integrate

```
template<class Type>
typename Foam::IntegrationScheme<Type>::integrationResult
Foam::Euler<Type>::integrate
(
    const Type& phi,
    const scalar dt,
    const Type& alphaBeta,
    const scalar beta
) const
{
    typename IntegrationScheme<Type>::integrationResult
retValue;
    retValue.value() = (phi + alphaBeta*dt)/(1.0 + beta*dt);
    retValue.average() = 0.5*(phi + retValue.value());

    return retValue;
}
```

A.4 Droplet evaporation during sensible heating process

When room-temperature aqueous urea is injected into the hot exhaust gas stream, the droplets are heated up to boiling point while evaporating water. Heat and mass exchange between a drop and the surrounding gas results temperature and concentration gradient in the drop. Rapid Mixing models ignore any gradients in a droplet assuming infinite fast transport in the liquid phase so that the droplet has homogenous temperature and properties. The variation of the urea concentration in the droplet can be described as follows with a non-volatile solute assumption for urea, i.e. $m_d Y_U$ is constant:

$$\dot{Y}_U = -\frac{\dot{m}_d}{m_d} Y_U \tag{A.23}$$

The mass change rate can be replaced by the rate of water vapor $\dot{m}_v = -\dot{m}_d$ due to the non-volatile urea assumption.

Droplet evaporation rate in the presence of vapor diffusion can be described through the Stefan flow analysis as (Sazhin, S.S. (2006); Birkhold et al. (2006)):

$$\frac{dm_d}{dt} = -\pi D_d \rho_g D_g Sh_0 \ln(1 + B_M) \tag{A.24}$$

Equation (A.24) is driven following widely accepted practices about density $\rho_{total} = \rho_g + \rho_v = \text{const} \approx \rho_g$ and diffusivity $D_g = D_v$ ②. The

② This assumption on diffusion coefficient is not quite right for water molecules in air. The coefficient of water in air is D=0.282 cm^2/s and that of oxygen in air is D=0.176 cm^2/s at 25℃, 1 atm. In case that the amount of water vaporization is large during sensible heating process,

Spalding mass and heat transfer numbers B_M and B_T are calculated as:

$$B_M = \frac{Y_{vs} - Y_{v\infty}}{1 - Y_{vs}} \tag{A.25}$$

$$B_T = \frac{c_{pv}\left(T_g - T_s\right)}{L - \left|\dot{q}_d\right| / \dot{m}_d} \tag{A.26}$$

Equation (A.11) based on energy balance analysis gives the relation between the Spalding mass and heat transfer numbers:

$$1 + B_T = \left(1 + B_M\right)^{\varphi} \tag{A.27}$$

$$\varphi = \frac{c_{pv}}{c_{pg}} \frac{Sh_0}{Nu_0} \frac{1}{Le_g} \tag{A.28}$$

where the Lewis number is $Le_g = \alpha / D = \left(k_g / \rho_g c_{pg}\right) / D_g$. Equation (A.27) holds for temperature away from boiling point since B_M diverges at such a condition. With the Reynolds number calculated by $Re = D_d \left|\vec{U}_d - \vec{U}_g\right| / \upsilon_g$ the Frossling correlations are used to evaluate the Nusselt and Sherwood numbers for a non-vaporizing droplet for forced convection:

$$Nu_0 = 2 + 0.552 Re^{1/2} Pr^{1/3} \tag{A.29}$$

$$Sh_0 = 2 + 0.552 Re^{1/2} Sc^{1/3} \tag{A.30}$$

Since those equations overestimate the transfer rate at low Reynolds number $Re \le 10$ it should be careful when dealing small drops with

---

Eq. (A.24) should be reexamined.

slow relative velocity. They are still widely used in practice. Note that some researchers prefer the coefficient 0.6 to 0.552.

For free convection, treating the Sherwood number is subtle since the analogy between heat and mass transfer from the same form of governing equations is broken. This is because the approach like the Boussinesq approximation is not applicable. It is not clear that free convection for mass transfer as well. The Sherwood number can still be assumed to be $Sh \cong 2$.

The heat transfer number Eq. (3.15) is written for a sensible heating process as follows:

$$B_T = \frac{c_{pv}(T_g - T_d)}{\Delta H - \frac{m_d c_{pd}}{\dot{m}_d}\frac{dT_d}{dt}} \tag{A.31}$$

or, the evolution of droplet temperature is:

$$\frac{dT_d}{dt} = -\frac{\dot{m}_d}{m_d c_{pd}}\left(\frac{c_{pv}(T_g - T_d)}{B_T} - \Delta H\right) \tag{A.32}$$

Equations (A.24) and (A.25) are governing equations for mass and heat transfer during a sensible heating process and the heat transfer number B_T of Eq. (A.26) is used from the mass transfer number defined in Eq. (A.25). If boiling point temperature is reached, another approach should be used to describe mass transfer since boiling phenomena is not confined to surface of the volume as in Eq. (A.24). Instead, mass transfer rate is determined by heat transfer from the surrounding gas.

For a mixture such as urea water solution, droplet evolution due to heat and mass transfer for a boiling process is described in Sec. 3.5. For pure substance, the boiling point temperature remains constant

unless surrounding pressure changes a lot. From energy balance mass transfer can be determined with the following equation:

$$\frac{dm_d}{dt} = -\pi D_d \frac{k_g}{cpv} Nu_0 \ln(1 + B_T) \tag{A.33}$$

with

$$B_T = \frac{c_{pv}(T_g - T_d)}{\Delta H} \tag{A.34}$$

Heat convection is considered by the Nusselt number such as the Frossling correlation Eq. (A.29).

A.5 Energy equation in OpenFOAM

Energy equation is used to calculate the status such as temperature and density of carrier flow where droplets travel. The energy equation comes from the law of conservation of energy that states the total energy of an isolated system remains constant. Energy contribution from mechanical and thermodynamic energy is considered in this section, and then the specific total energy due to internal and kinetic energy is as:

$$E = e + K = e + \frac{\vec{u} \cdot \vec{u}}{2} \tag{A.35}$$

The energy change of an isolated system from the first law of thermodynamics says:

$$\frac{D}{Dt}\int dV\rho(e+K) = -\int d\vec{A}\cdot\vec{q} + \int d\vec{A}\cdot\vec{\vec{\sigma}}\cdot\vec{u} \tag{A.36}$$

The stress tensor $\vec{\vec{\sigma}} = -p\vec{\vec{I}} + \vec{\vec{\tau}}$ with Eq. (A.36) gives:

$$\frac{D}{Dt}\int dV\rho(e+K) + \int d\vec{A}\cdot\rho\vec{u}\left(\frac{p}{\rho}\right) = -\int d\vec{A}\cdot\vec{q} + \int d\vec{A}\cdot\vec{\vec{\tau}}\cdot\vec{u} \tag{A.37}$$

Plug zero $0 = \int dV \frac{\partial}{\partial t}\left(\rho\frac{p}{\rho}\right) - \int dV \frac{\partial}{\partial t}\left(\rho\frac{p}{\rho}\right)$ into the left hand side of Eq. (A.37) and use the enthalpy relation with the internal energy $h = e + \frac{p}{\rho}$, then Eq. (A.37) can be written as in differential form:

$$\frac{\partial \rho(h+K)}{\partial t} + \nabla \cdot [\rho \vec{u}(h+K)] - \frac{\partial p}{\partial t} + \nabla \cdot q = \nabla \cdot \left(\vec{\vec{\tau}} \cdot \vec{u}\right) \quad \text{(A.38)}$$

The energy equation (A.38) is implemented without the mechanical source $\nabla \cdot \left(\vec{\vec{\tau}} \cdot \vec{u}\right)$ since its influence is negligible unless there is a rapid change such as shock wave. A heat flux $\vec{q} = -\alpha_{eff} \nabla e$ is assumed where the effective thermal diffusivity includes the thermal diffusivity depending on the condition of carrier flow. For example, an energy equation for compressible solvers in OpenFOAM has the following implementation:

Code A.3 EEqn.H

```
volScalarField& he = thermo.he();

fvScalarMatrix EEqn
(
    fvm::ddt(rho, he) + fvm::div(phi, he)
    + fvc::ddt(rho, K) + fvc::div(phi, K)
    + (
          he.name() == "e"
        ? fvc::div
          (
              fvc::absolute(phi/fvc::interpolate(rho), U),
              p,
              "div(phiv,p)"
          )
        : -dpdt
       )
    - fvm::laplacian(turbulence->alphaEff(), he)
    ==
    fvOptions(rho, he)
);
```

Appendix B

B.1 Arduino-Uno master code for experiments

The Arduino-Uno is a microcontroller board and it has 14 digital input/output pins of which 6 can be used as Pulse Width Modulation (PWM) outputs, 6 analog inputs.

There are three k-type thermocouples used in the experiment for temperature monitor and LM35 used for checking the surrounding temperature around the board. To prevent from overheating the beaker mantle, temperatures at two spots inside the mantle and right below the beaker are monitored and the sample temperature is monitored as well. To control the temperature of the mantle solid-state relay is used and the temperature is controlled by the PWM method. To prevent the temperature overshoot of the reactor a fan is installed above the reactor and a relay is used too. Data are gathered in a laptop via USB cable. Source code building and uploading is done on a laptop.

Master code for experiments is listed following pages. Temperature monitor for the experiments of boiling-point elevation is done by a slightly modified this code in code B.1.

Code B.1 arduino_controller.ino

```
#include <math.h>
#include <PID_v1.h>
#include <SimpleTimer.h>

double setPoint;
double setPointY1, setPointY2;

SimpleTimer timer;

double voltage5 = 4.8;

struct IC595 {
  int pin;
  int val;
  double temp;
} amp;

struct IC35 {
  int pin;
  int val;
  double temp;
} board;

struct IC4051 {
  int Ebar;
  int S0;
  int S1;
  int val;
  double Y0;
  double Y1;
  double Y2;
} mux;

struct ULN2003 {
  int fan;
  int mandtl;
} ssr;


void RepeatTask()
{
  //Serial.print(".....................5 second timer:
");
  ClockDisplay();
  //unsigned long timec = millis();
  getTempETC();
  getY0Y1Y2();
  //Serial.println(millis()-timec);
  Serial.print(",\t");
  Serial.print(board.temp);
  Serial.print(",\t");

  Serial.print(mux.Y0);
  Serial.print(",\t");
  Serial.print(mux.Y1);
  Serial.print(",\t");
  Serial.println(mux.Y2);
}

void ClockDisplay()
{
  int s = millis()/1000;
```

```
  Serial.print(s);
}

void getTempETC()
{
  //Serial.print("\n\nLM35: ");
  board.val = analogRead(board.pin);
  board.temp = LM35ToTemp(board.val);
}

void getY0Y1Y2()
{
  digitalWrite(mux.S1, LOW); digitalWrite(mux.S0, LOW);
delay(10);
  digitalWrite(mux.Ebar, LOW); delay(10);
  amp.val = analogRead(amp.pin);
  amp.temp = AD595ToTemp(amp.val);
  mux.Y0 = amp.temp;
  digitalWrite(mux.Ebar, HIGH); delay(100);

  digitalWrite(mux.S1, LOW); digitalWrite(mux.S0, HIGH);
delay(10);
  digitalWrite(mux.Ebar, LOW); delay(10);
  amp.val = analogRead(amp.pin);
  amp.temp = AD595ToTemp(amp.val);
  mux.Y1 = amp.temp;
  digitalWrite(mux.Ebar, HIGH); delay(100);

  digitalWrite(mux.S1, HIGH); digitalWrite(mux.S0, LOW);
delay(10);
  digitalWrite(mux.Ebar, LOW); delay(10);
  amp.val = analogRead(amp.pin);
  amp.temp = AD595ToTemp(amp.val);
  mux.Y2 = amp.temp;
  digitalWrite(mux.Ebar, HIGH); delay(100);
}

double AD595ToTemp(int val)
{
  double x, temp;
  x = (double)val*4.8/1.024;
  temp = 0.0990833607*x;
  return temp;
}

double LM35ToTemp(int val)
{
  return (double)val*voltage5/1.024/10.0;
}

void setup()
{
  /*
  thermistor.pin = A0;
  thermistor.val = 0;
  thermistor.temp = 0.0;
  */

  amp.pin  = A5;
  amp.val  = 0;
  amp.temp = 0.0;

  board.pin  = A3;
  board.val  = 0;
  board.temp = 0.0;
```

```
  mux.Ebar = 9;
  mux.S0   = 8;
  mux.S1   = 7;

  ssr.fan    = 6;
  ssr.mandtl = 5;

  pinMode(mux.S0, OUTPUT);
  digitalWrite(mux.S0, LOW);
  pinMode(mux.S1, OUTPUT);
  digitalWrite(mux.S1, LOW);
  pinMode(mux.Ebar, OUTPUT);
  digitalWrite(mux.Ebar, HIGH);

  pinMode(ssr.fan, OUTPUT);
  digitalWrite(ssr.fan, LOW);
  pinMode(ssr.mandtl, OUTPUT);
  //digitalWrite(ssr.mandtl, LOW);

  Serial.begin(9600);

  setPointY2 = 200.0;
  setPointY1 = 180.0;
  setPoint   = setPointY2;

Serial.println("SEC\tLM35\tY0(INT)\tY1(TOP)\tY2(BOT)");
  timer.setInterval(5000, RepeatTask);
}

void loop()
{
  double err = 0.0;
  double pwmfac = 0.4;
  //double tempCrt;
  timer.run();

  if (mux.Y1<150.0) {
    if (mux.Y2-setPointY2>0.0) {
      pwmfac = 0.0;
    } else if (setPointY2-mux.Y2<4.0) {
      pwmfac = 0.14;
    } else {
      pwmfac = 0.55;
    }
  } else {
    err = setPointY1 - mux.Y1;
    //double yintercept = 0.11; // for T = 170
    double yintercept = 0.12; // for T = 180
    if (err>0) {
      pwmfac = (0.22-yintercept)/10.0*err + yintercept;
    } else {
      pwmfac = yintercept*(err/5.0 + 1.0);
    }

    if (pwmfac > 0.35) {
      pwmfac = 0.35;
    } else if (pwmfac < 0.0) {
      pwmfac = 0.0;
    }
  }

  analogWrite(ssr.mandtl, 255.0*pwmfac);
}
```

B.2 Octave code for urea pyrolysis

The two-step method described in chapter 2 is implemented in the subroutine **pyrolysis_urea.m** of Code B.2. The number of moles of each species is stored in the columns of variables. Urea, isocyanic acid, biuret, cyauric acid, evaporated ammonia and evaporated isocyanic acid are stored at the first column, the second column etc.

The chemical kinetics and evaporation are solved in the normalized equation and the explicit Euler method is chosen as a time marching step.

Code B.2 pyrolysis_urea.m

```
global k1
global k3
global be
global Ae

function ndot=f(n,t)
global k1
global k3
global be
global Ae
ndot=zeros(6,1);
nu=n(1);
ni=n(2);
nb=n(3);
nc=n(4);
nae=n(5);
nie=n(6);
if nu<1e-7
   nu=1e-7;
   n(1)=1e-7;
end
if nb<1e-7
   nb=1e-7;
   n(3)=1e-7;
end
nt=sum(n);
fdel=(1/nt-1/nu)*(-k1*nu)+1/nb*(-k3*ni*nb/nt);
fdel=fdel+(1/nt-1/ni)*(k1*nu-Ae*be*ni/nt-k3*ni*nb/nt);
fdel=-fdel/(1/nb+1/nu+1/ni-1/nt);
ndot(1)=-k1*nu-fdel;
ndot(2)=k1*nu-Ae*be*ni/nt-k3*ni*nb/nt-fdel;
ndot(3)=-k3*ni*nb/nt+fdel;
ndot(4)=k3*ni*nb/nt;
ndot(5)=k1*nu+k3*ni*nb/nt;
ndot(6)=Ae*be*ni/nt;
endfunction

T=273+200;
Ea1=7.6918E+04
Ea3=1.4356E+05
A1=2.5021E+05
A3=2.7020E+13
B=1.1987E+01

R=8.3145;
k1=A1*exp(-Ea1/R/T);
k3=A3*exp(-Ea3/R/T);
```

```
dH=20.6e3;
be=B/sqrt(T)*exp(-dH/R/T);
Ae=7.69*0.02*1; %20g
%Ae = 70e-3^2*pi/4

n0=[0.3321; 5.047e-4; 5.047e-4; 0; 0; 0];

t=linspace(0, 8000, 8001);
n=lsode("f", n0, t);
msol=n(:,1)*60 + n(:,2)*43 + n(:,3)*103 + n(:,4)*129;
meva=n(:,5)*17 + n(:,6)*43;

nU0=n(1,1);
n=n/nU0;
msol = msol / 20;
meva = meva / 20;
subplot(2,1,1)
plot(t,n(:,1),t,n(:,2),t,n(:,3),t,n(:,4))
subplot(2,1,2)
plot(t,n(:,5),t,n(:,6))
%csvwrite('t200_10.csv', [t; n'; msol'; meva']');
%
%plot(t,msol, t,n(:,4)*103)
%cya=n(end,4)*103
```

```
%csvwrite('history.csv', [t; n']')
```

B.3 Octave code for water vaporization from an aqueous droplet due to free convection

Octave handles ordinary differential equations of the form

$$\frac{dx}{dt} = f(x,t) \tag{B.1}$$

using a built-in function *[x, istate, msg] =* lsode *(fcn, x_0, t)* with *x(t_0) = x_0*. The solution is returned in the matrix x, with each row corresponding to an element of the vector t. In the main code, the lsode is called m=lsode("dmf", [mU0/0.325], t) to solve the ordinary differential equation for drop mass in Eq. (2.19) implemented in the routine dmf and the required boiling-point elevation and its derivative routines are defined in the routines elev(x) and delev(x). Air properties are supplied in a separate file air_prop.csv to deal with the variation of air properties according to the change of droplet temperature.

Code B.3 droplet_free_convection.m

```
%graphics_toolkit('gnuplot')
clear all

function delT=elev(x)
        R=8.3145;
        Tnbp=100+273.15;
        delH=40.7e3;
        delT=-R*Tnbp*log(1-x)./(delH/Tnbp+R*log(1-x));
endfunction

function ddelT=delev(x)
        h=0.001;
        ddelT=(elev(x+h)-elev(x-h))/(2*h);
endfunction

function dm=dmf(m,t)
        global Tg
        global mU0
        dm=zeros(1,1);

   Tnbp = 100+273;
        g=9.81;
        cpv=1976; %473K
        %{
        be=2.43e-3;
        al=0.03965e-3;
        nu=27.55e-6;
        kg=0.0343;
        Pr=0.695;
        %}
        MWMU=18/60;
        YU=mU0/m;
        cD=4200*(1-YU)+3000*YU; %drop
        rhoD=950*(1-YU)+1300*YU; % drop
        rD=cbrt(m/(rhoD*4*pi/3));
        DD=2*rD;
        %x=(m/mU0-1)/MWMU+1;
        %x=1./x;
YW = 1 - YU;
nT = m*YW/18 + m*YU/60;
x = m*YU/60/nT;
        %[x,elev(x)]
        airt=csvread("air_prop.csv"); % celcius
        Td=Tnbp+elev(x);
        airp=interp1(airt(:,1)+273,airt,(Tg+Td)/2, 'extrap');
        be=airp(6)*1e-3;
        al=airp(8)*1e-3;
```

```
        nu=airp(5)*1e-6;
        kg=airp(4);
        Pr=airp(7);

        dqdm1=(40.7e3-2.2e3)/0.018;
        dqdm2=m*cD*delev(x)*x^2/MWMU/mU0;
        dqdm=dqdm1+dqdm2;
        BT=cpv*(Tg-Td)/dqdm;
        RaDD=g*be*(Tg-Td)*DD.^3/nu/al;
        NuDD=2+0.589*RaDD.^(1/4)/(1+(0.469/Pr)^(9/16))^(4/9);
        dm=-pi*DD*kg/cpv*NuDD*log(1+BT);
        if (YU>0.95)
      t
        endif

endfunction

function [x,T,rD]=postode(m)
        global mU0
        MWMU=18/60;

        YU=mU0./m;
        cD=4200*(1-YU)+3000*YU; %drop
        rhoD=950*(1-YU)+1300*YU; % drop
        rD=(m./(rhoD*4*pi/3)).^(1/3);
        DD=2*rD;
    YW = 1 - YU;
    nT = m.*YW/18 + m.*YU/60;
    x = m.*YU/60./nT;
        %x=(m./mU0-1)/MWMU+1;
        %x=1./x;
        T=elev(x);
endfunction

global Tg
global mU0


%Wang
Tg=200+273.15;
DD0=0.87e-3;
tend=44*(DD0*1000)^2
%tend=85

RD0=DD0/2;
YU=0.325;
rhoD=950*(1-YU)+1300*YU; % drop
m0=rhoD*4*pi/3*RD0^3;
mU0=rhoD*4*pi/3*RD0^3*YU;
```

```
tsize = 1000
t=linspace(0,tend,tsize);
mrk4=zeros(size(t));
mrk4(1)=m0;
h=t(2);
for n=2:tsize
   mn = mrk4(n-1);
   tn = t(n-1);
   k1=h*dmf(mn, tn);
   k2=h*dmf(mn+k1/2, tn+h/2);
   k3=h*dmf(mn+k2/2, tn+h/2);
   k4=h*dmf(mn+k3, tn+h);
   mrk4(n) = mn + k1/6+(k2+k3)/3+k4/6;
endfor

[x,T,rD]=postode(mrk4);

t=t/(DD0*1000)^2;
subplot(3,1,1)
%plot(t/(DD0*1000)^2, mrk4/m0)
plot(t, mrk4/m0)
subplot(3,1,2)
plot(t, T)
subplot(3,1,3)
plot(t, x)

Tsample = [105, 110, 120, 130, 150]';
sample = interp1(T'+100, [t;T+100;mrk4/m0]', Tsample);
sample = [0, T(1)+100, 0; sample]
```

air_prop.csv

```
-150,2.793,1.026,0.0116,3.08,8.21,0.76,0.0040479924
-100,1.98,1.009,0.016,5.95,5.82,0.74,0.0080087295
-50,1.534,1.005,0.0204,9.55,4.51,0.725,0.0132324038
0,1.293,1.005,0.0243,13.3,3.67,0.715,0.0187000035
20,1.205,1.005,0.0257,15.11,3.43,0.713,0.0212216924
40,1.127,1.005,0.0271,16.97,3.2,0.711,0.0239265077
60,1.067,1.009,0.0285,18.9,3,0.709,0.0264721536
80,1,1.009,0.0299,20.94,2.83,0.708,0.0296333003
100,0.946,1.009,0.0314,23.06,2.68,0.703,0.0328963221
120,0.898,1.013,0.0328,25.23,2.55,0.7,0.0360568731
140,0.854,1.013,0.0343,27.55,2.43,0.695,0.0396485039
160,0.815,1.017,0.0358,29.85,2.32,0.69,0.0431921144
180,0.779,1.022,0.0372,32.29,2.21,0.69,0.0467255677
200,0.746,1.026,0.0386,34.63,2.11,0.685,0.0504314107
250,0.675,1.034,0.0421,41.17,1.91,0.68,0.0603195071
300,0.616,1.047,0.0454,47.85,1.75,0.68,0.0703928354
350,0.566,1.055,0.0485,55.05,1.61,0.68,0.0812218445
400,0.524,1.068,0.0515,62.53,1.49,0.68,0.0920247591
```

B.4 OpenFOAM code for water vaporization from an aqueous droplet

To reuse the existing OpenFOAM code, members from kinematic and thermal parcels are derived when developing basicUreaWaterParcel class. The inheritance is defined in Code B.4. The detailed implementation should be consulted the raw source code. The core code for the proposed model of heating and evaporating water is implemented in Code B.5 where dropstate_ has the status of droplet and controls the flows.

Code B.4 basicUreaWaterCloud.H

```
#ifndef basicUreaWaterCloud_H
#define basicUreaWaterCloud_H

#include "Cloud.H"
#include "KinematicCloud.H"
#include "ThermoCloud.H"
#include "ReactingCloud.H"
#include "basicUreaWaterParcel.H"

namespace Foam
{
    typedef ReactingCloud
    <
        ThermoCloud
        <
            KinematicCloud
            <
                Cloud
                <
                    basicUreaWaterParcel
                >
            >
        >
    > basicUreaWaterCloud;
}
```

Code B.5 Foam::UreaWaterParcel<ParcelType>::calc

```
template<class ParcelType>
template<class TrackData>
void Foam::UreaWaterParcel<ParcelType>::calc
(
    TrackData& td,
    const scalar dt,
    const label cellI
)
{
    typedef   typename   TrackData::cloudType::reactingCloudType
reactingCloudType;
    const CompositionModel<reactingCloudType>& composition =
        td.cloud().composition();


    // Define local properties at beginning of time step
    // ~~~~~~~~~~~~~~~~~~~~~~~~~~~~~~~~~~~~~~~~~~~~~~~~~~~~~

    const scalar np0 = this->nParticle_;
    const scalar d0 = this->d_;
    const vector& U0 = this->U_;
    const scalar T0 = this->T_;
    const scalar mass0 = this->mass();

    massU_ = mass0 * Y_[1];

    // Calc surface values
    scalar Ts, rhos, mus, Prs, kappas;
    this->calcSurfaceValues(td, cellI, T0, Ts, rhos, mus, Prs,
kappas);
    scalar Res = this->Re(U0, d0, rhos, mus);


    // Sources
    //~~~~~~~~~
    // Explicit momentum source for particle
    vector Su = vector::zero;
    // Linearised momentum source coefficient
    scalar Spu = 0.0;
    // Momentum transfer from the particle to the carrier phase
    vector dUTrans = vector::zero;
    // Explicit enthalpy source for particle
    scalar Sh = 0.0;
    // Linearised enthalpy source coefficient
    scalar Sph = 0.0;
    //  Sensible  enthalpy  transfer  from  the  particle  to  the
carrier phase
    scalar dhsTrans = 0.0;

    // Mass transfer due to phase change
    scalarField dMassPC(Y_.size(), 0.0);

    //  Molar  flux  of  species  emitted  from  the  particle
(kmol/m^2/s)
```

```
   //scalar Ne = 0.0;

   // Sum Ni*Cpi*Wi of emission species
   scalar NCpW = 0.0;

   // Surface concentrations of emitted species
   scalarField Cs(composition.carrier().species().size(), 0.0);

   scalarField dMass(dMassPC);
   scalar mass1 = updateMassFraction(mass0, dMass, Y_);

   correctSurfaceValues(td, cellI, Ts, Cs, rhos, mus, Prs,
kappas);
   Res = this->Re(U0, this->d_, rhos, mus);

   //Info << "........................................." <<
endl;



   /*
   if (mass0 < 1e-15) {
      std::cout << "mass0: " << mass0 << std::endl;
      return;
   }
   */

   switch ( dropState_ ) {
      case InitTran:
```

```
         {
            scalar Tn = this->T_;
            scalarField xn(Y_);
            xn[0] = Y_[0]/MW_[0];
            xn[1] = Y_[1]/MW_[1];
            scalar nT = sum(xn); // note that actual amount
of molecules is nT*mass
            xn[0] = xn[0]/nT;
            xn[1] = xn[1]/nT;
            //std::cout << "Yn:( " << Y_[0] << ", " << Y_[1]
<< " )" << std::endl;
            //std::cout << "xn:( " << xn[0] << ", " << xn[1]
<< " )" << std::endl;
            scalar delH = delHnbp_ * pow((Tcri_-Tn)/(Tcri_-
Tnbp_), 0.38);
            scalar Tbp = R_*log(xn[0])/delH + 1./Tnbp_;
            Tbp = 1./Tbp;

            this->T_ =
               this->calcHeatTransfer (
                     td,
                     dt,
                     cellI,
                     Res,
                     Prs,
                     kappas,
                     NCpW,
                     Sh,
```

```
                        dhsTrans,
                        Sph
                        );
            // if T_ > Tbp then, T_ <- Tbp, save drop age,
            if (this->T_ > Tbp) {
               dropState_ = WaterEvap;
               this->T_ = Tbp;

               std::ofstream boilStart;
               boilStart.open("boilStart.dat",
std::fstream::out | std::fstream::app);
               boilStart << massU_ << ", " << this->age_ <<
std::endl;
               boilStart.close();
            }


         } break;

      case WaterEvap:
         {

            if (Y_[1] > 0.95) {
               break;
            }
            // RK2
            // temporal variables
            //
            // n+1/2
            scalar Tn = this->T_;
            scalarField Yn(Y_);
            scalarField xn(Y_);
            scalar massn = mass0;
            scalar dn = d0;

            xn[0] = Y_[0]/MW_[0];
            xn[1] = Y_[1]/MW_[1];
            scalar nT = sum(xn); // note that actual amount
of molecules is nT*mass
            xn[0] = xn[0]/nT;
            xn[1] = xn[1]/nT;

            scalar delH = delHnbp_ * pow((Tcri_-Tn)/(Tcri_-
Tnbp_), 0.38);
            scalar delHp = delH + delHdis_;
            scalar cdn = 4200.0*Yn[0] + 3000.0*Yn[1];
            scalar                    qm                    =
massn*cdn*Tn*Tn*R_/delH/xn[0]*MW_[1]/MW_[0]*xn[1]*xn[1]/massU_;
            qm = qm + delHp/0.018; // J/kg
            scalar BT = 1./qm*1900.0*(this->Tc_ - Tn); //
1900 from cpv, need to modify
            this->calcSurfaceValues(td, cellI, Tn, Ts, rhos,
mus, Prs, kappas);
            Res = this->Re(U0, dn, rhos, mus);
            scalar Nu0 = 2.0 + 0.6*sqrt(Res)*cbrt(Prs);
            scalar         delmassn         =         dt/2.0*(-
```

```
constant::mathematical::pi*dn*kappas/1900.0);
            delmassn = delmassn*Nu0*log(1.0+BT);
            //std::cout << "massn,del,ratio: (" << massn <<
"," << delmassn;
            //std::cout << "," << massn/delmassn << ") dt: "
<< dt << std::endl;

            // update YU0, xU0, md0, Dd0, preparing n
            scalar massn1half = massn + delmassn;
            Yn[1] = massU_/massn1half;
            Yn[0] = 1.0 - Yn[1];

            xn[0] = Yn[0]/MW_[0];
            xn[1] = Yn[1]/MW_[1];
            nT = sum(xn); // note that actual amount of
molecules is nT*mass
            xn[0] = xn[0]/nT;
            xn[1] = xn[1]/nT;

            Tn = R_*log(xn[0])/delH + 1./Tnbp_;
            Tn = 1./Tn;
            scalar rhodn = 950.0*Yn[0] + 1300.0*Yn[1];
            dn                                              =
cbrt( 6.0*massn/constant::mathematical::pi/rhodn );

            // n
            delH = delHnbp_ * pow((Tcri_-Tn)/(Tcri_-Tnbp_),
0.38);
            delHp = delH + delHdis_;
            cdn = 4200.0*Yn[0] + 3000.0*Yn[1];
            qm                                              =
massn*cdn*Tn*Tn*R_/delH/xn[0]*MW_[1]/MW_[0]*xn[1]*xn[1]/massU_;
            qm = qm + delHp/0.018;
            BT = 1./qm*1900.0*(this->Tc_ - Tn);
            this->calcSurfaceValues(td, cellI, Tn, Ts, rhos,
mus, Prs, kappas);
            Res = this->Re(U0, dn, rhos, mus);
            Nu0 = 2.0 + 0.6*sqrt(Res)*cbrt(Prs);
            delmassn                  =                  dt*(-
constant::mathematical::pi*dn*kappas/1900.0);
            delmassn = delmassn*Nu0*log(1.0+BT);

            // update YU0, xU0, md0, Dd0 and related class
variables
            //
            // if YU0 > 0.95, save time etc
            massn = massn + delmassn;
            Yn[1] = massU_/massn;
            Yn[0] = 1.0 - Yn[1];

            xn[0] = Yn[0]/MW_[0];
            xn[1] = Yn[1]/MW_[1];
            nT = sum(xn); // note that actual amount of
molecules is nT*mass
            xn[0] = xn[0]/nT;
            xn[1] = xn[1]/nT;
```

```
            if (Yn[1] > 0.95) {
                massn = massU_;
                dropState_ = UreaDrop;
                Yn[0] = 0.05;
                Yn[1] = 0.95;
                xn[0] = Yn[0]/MW_[0];
                xn[1] = Yn[1]/MW_[1];
                nT = sum(xn); // note that actual amount of
molecules is nT*mass
                xn[0] = xn[0]/nT;
                xn[1] = xn[1]/nT;

                Tn = R_*log(xn[0])/delH + 1./Tnbp_;
                Tn = 1./Tn;

                std::ofstream boilEnd;
                boilEnd.open("boilEnd.dat",   std::fstream::out
| std::fstream::app);
                boilEnd << massU_ << ", " << this->age_ <<
std::endl;
                boilEnd.close();
            } else {
                xn[0] = Yn[0]/MW_[0];
                xn[1] = Yn[1]/MW_[1];
                nT = sum(xn); // note that actual amount of
molecules is nT*mass
                xn[0] = xn[0]/nT;
                xn[1] = xn[1]/nT;

                Tn = R_*log(xn[0])/delH + 1./Tnbp_;
                Tn = 1./Tn;
            }
            rhodn = 950.0*Yn[0] + 1300.0*Yn[1];
            dn                                                  =
cbrt( 6.0*massn/constant::mathematical::pi/rhodn );
            cdn = 4200.0*Yn[0] + 3000.0*Yn[1];

            Y_[0] = Yn[0];
            Y_[1] = Yn[1];
            //std::cout << "Y: " << Y_[0] << "," << Y_[1] <<
std::endl;
            this->T_ = Tn;
            this->d_ = dn;
            this->Cp_ = cdn;
            this->rho_ = rhodn;
            this->mass0_ = massn;

        }
        break;

    case UreaDrop:

        break;
   }
//<-------------------------snip
```

선택적 촉매 환원법을 위한 요소수용액의 증발과 분해 연구

서울대학교 대학원

기계항공공학부

기계항공공학전공

단 호 진

요 약

대기 오염은 환경과 건강에 큰 영향을 미치고 있다. 이 오염을 일으키는 중요한 발생원으로 화석연료를 이용하는 내연 기관을 들 수 있다. 특히 차량의 밀집도가 높은 도시에서 큰 문제가 되고 있으며, 세계 각국에서는 대기가스배출 규제를 마련하여 이에 대응하고 있다. 디젤엔진의 고온 연소에서 발생하는 질소산화물은 대기로 배출되면 산성비나 도시에서의 광화학스모그를 일으킬 수 있어 중요 관리 대상으로 분류되어 있다. 엔진 제조사들은 강화되는 질소산화물 규제에 대응하기 위하여 기술을 개발하고 있으며, 요소 이용 선택적 촉매 환원 기법(Urea-SCR technology)은 가장 현실적인 기술로 평가 받고 있다.

요소 수용액을 사용하는 석택적 촉매 환원 기술은 배기 유로에서 요소 수용액을 촉매에서 환원제로 사용되는 암모니아로 전환되어야 한다. 이 전환 과정은 물의 증발, 요소의 열분해와 이소시안산의 가수분해를 거쳐 암모니아로 전환된다. 이 과정은 요소수용액을 배기 유로에 분무하는 것으로 시작된다. 이중 일부 요소수용액의 액적은 내부 면에 도달하여 퇴적물질을 남길 수가 있다. 본 연구는 이 퇴적 현상을 이해하는데 필요한 물질 특성에 관한 기초 연구로 장기적으로 퇴적을 일으키는 화학 반응에 대한 연구와 요소수용액의 총괄성질(colligative property)에 관한 연구로

나뉘어 있다.

요소 이용 선택적 촉매 환원 기법 시스템에서 요소 분해 부산물의 퇴적은 주로 200℃ 근방의 온도에서 일어난다. 본 연구에서는 이 온도에서 발생하는 요소의 분해 모형을 제시하였다. 이 온도 근방에서는 요소, 이소시안산, 뷰렛, 시아누르산, 그리고 암모니아가 화학 반응에 참여하는 주요 분자이며, 이 분자들간의 화학 반응 모델을 제안하였다. 시아누르산은 복잡한 중합체가 형성하는데 기본 재료로 사용되며 고온에서만 분해되어 퇴적물 형성의 핵심이 되는 분자이다. 따라서 퇴적 현상을 이해하기 위해서는 시아누르산의 형성 모형을 규명하는 것이 필요하다. 다섯 가지 분자간의 화학 반응을 제안하였고, 아레니우스 식과 분출(effusion)식을 이용하여 화학반응 속도 관계를 구성하였다. 빠른 화학반응을 화학평형으로 가정한 과도식을 구성하여 반응 모델을 수립하였다. 모형에 필요한 물리상수를 얻기 위하여 개방형 반응기에서 시료의 질량 변화를 측정하였고, 제안된 모델과의 오차가 최소가 되는 상수를 찾았다. 요소의 분해에 관한 상수를 기존 연구자들의 결과와 비교하여 제안된 모델이 유효함을 보였다. 제안된 모델을 이용하여 시아누르산의 형성과 이소시안산의 증발의 경합 관계를 살펴보았으며 온도가 낮은 경우에 퇴적이 더 크게 형성될 수 있음을 보였다.

물의 증발은 요소가 암모니아로 전환되는데 있어 가장 최초의 과정이다. 배기 유로에 분무된 요소수 액적은 비휘발성 요소는 용질로 물 용매에 녹아있다고 볼 수 있다. 물의 증발이 진행되면 용액에 상대적인 잔존 비율이 달라지며 이런 비율은 액적의 열·물리적인 성질을 변화시킨다. 이를 총괄성이라고 한다. 물의 증발에서 중요하게 관련있는 성질은 끓는점오름과 증발열변화이다. 본 연구를 통하여 고농도의 요소가 녹아있는 경우 끓는점오름이 어떻게 될 것인지 제안하였고, 실험을 통하여 그 관계가 유효함을 보였다. 외기에서 열이 들어올 때 이 에너지가 증발, 증기의 가열, 액적의 가열에 어떻게 배분되는지를 끓는점 오름 맥락에서 보였다. 이때 요소의 융해열이 역으로 물의 증발에 어떻게 영향을 주는지 고찰하였으며 실험을 통하여 제안한 보정 값이 유효함을 보였다. 제안된 끓는점오름과 기화열보정을 액적의 거동에 적용하여 열전달 모델이 타당함을 보였다. 액적 해석을 통하여 물의 증발 말기에 액적의 온도는

요소의 분해가 시작될 정도의 온도까지 오르는 것을 보였다. 벽면에 액적이 도달하여 에너지를 전달하고, 침전 현상이 진행될 때 이 액적의 온도가 중요하므로 요소 활용 선택적 촉매 환원 시스템의 해석에 핵심적으로 활용될 것으로 기대한다.

주요어: 선택적 촉매 환원, 요소 열해리, 물증발, 시안산, 끓는점오름, 증발열

학번: 2012-30170